Garbarino, Nicola

Working Paper

Concrete adaptation under extreme precipitation

ifo Working Paper, No. 419

Provided in Cooperation with:
Ifo Institute – Leibniz Institute for Economic Research at the University of Munich

Suggested Citation: Garbarino, Nicola (2025) : Concrete adaptation under extreme precipitation, ifo Working Paper, No. 419, ifo Institute - Leibniz Institute for Economic Research at the University of Munich, Munich

This Version is available at:
https://hdl.handle.net/10419/331806

ifo Working Papers

419
2025

October 2025

Concrete Adaptation under Extreme Precipitation

Nicola Garbarino

ifo Institute
Leibniz Institute for
Economic Research at the
University of Munich

Imprint:

ifo Working Papers

Publisher and distributor: ifo Institute – Leibniz Institute
for Economic Research at the University of Munich

Poschingerstr. 5 | 81679 Munich, Germany

Telephone + 49(0)89 9224 0
Telefax +49(0)89 985369, email ifo@ifo.de

https://www.ifo.de

Concrete Adaptation under Extreme Precipitation

Nicola Garbarino*

Abstract

Does land development adapt to changing climate risks? Extreme precipitation increases flood risk, yet land-use decisions may overlook rare events. Drawing on nearly half a century of climate and land-use data for Europe (1975–2020), this paper finds that extreme precipitation slows the expansion of built-up areas, though only slightly. The effect is stronger over longer horizons, consistent with a clearer climate signal. Adaptation is concentrated in fast-growing urban areas. An accounting framework that combines these effects suggests that relocation in response to shifting precipitation patterns has reduced damages by roughly 5%.

*ifo Institute and LMU Munich. Email: garbarino@ifo.de. I thank Maximilian Auffhammer, João Cocco, Maximilian Kotz, Christian Lessner, Manuel Linsenmeier, Filippo Pavanello, Karen Pittel, Lorenzo Sileci, Marcel Thum, Christian Traeger, and Maria Waldinger for valuable comments. Financial support from the German Federal Ministry of Research, Technology and Space (grant no. 01LR2006C) is gratefully acknowledged.

1 Introduction

Over the past century, extreme precipitation has become more frequent and more intense, and the trend is expected to continue (Myhre et al., 2019). Historically, local climate has influenced the distribution of human settlements (Henderson et al., 2018). How will the increase in extreme precipitation shape the growth of cities, towns and villages?

On the one hand, there are good reasons to reduce the construction of long-term real estate assets in areas exposed to extreme precipitation. Avoiding higher risk areas should limit both direct flood damage (Frame, 1998) and other negative effects on local growth (Kotz et al., 2022). On the other, flood plains are being developed at a rapid pace (Rajib et al., 2023) and risk does not appear to be fully priced in property markets (Hino and Burke, 2021). Possible explanations include public investment in flood protection (Hsiao, 2023), optimistic risk perceptions (Bakkensen and Barrage, 2022), climate scepticism (Bernstein et al., 2022), the benefits of existing urban agglomerations (often close to rivers and coasts, Lin et al. (2024)), and urban planning that pushes development towards unregulated high-risk areas (Ospital, 2023).

This paper estimates the effect of extreme precipitation on land development in Europe over nearly half a century (1975–2020), following the literature on climate damages and adaptation (Hsiang, 2016; Auffhammer, 2018; Carleton et al., 2024). The main finding is that extreme precipitation slows the expansion of built-up areas, with effects becoming apparent only over longer horizons as climate signals emerge more clearly. The extent of this adaptation is however modest and contributes little to offsetting the damage from more frequent extreme precipitation.

Precipitation data are comprehensive across time and space, and local rainfall is unlikely to be influenced by local building decisions.[1] Extreme precipitation is nevertheless an imperfect proxy for flood risk, since many events cause no damage and floods may originate from rainfall elsewhere in a river's basin. To strengthen the analysis, the paper also uses data on major hydrological disasters, which provide an independent measure to link extreme precipitation and flood damage. These records capture only large events and may still be influenced by the extent of built-up land, but they offer an important validation of the damage channel.[2]

[1] Reverse causality cannot, however, be entirely ruled out: large-scale deforestation or reforestation can affect local precipitation patterns (Grosset et al., 2023). See Taylor and Druckenmiller (2022) for evidence on land use and flood risk.

[2] See Faiella et al. (2020) for an overview of disaster datasets.

The analysis combines land-use and weather data for Europe at 0.1° resolution (cells of about 55–90 km^2, depending on latitude). Land development is measured as the share of each cell covered by buildings at five-year intervals from 1975 to 2020. Extreme precipitation is defined as the annual average number of days with rainfall above the 99.9^{th} percentile of each cell's daily precipitation distribution. For the damage analysis, these data are aggregated to the NUTS-3 level (local administrative regions) and matched with records of major hydrological events in Europe since 1980.[3]

Both built-up area and the frequency of extreme precipitation have increased markedly in Europe over recent decades. The average built-up share rose from 0.44% of cell surface in 1975 to 0.82% in 2020, while the average number of days above the 99.9^{th} percentile of daily precipitation grew from 0.31 to 0.48 per year.[4] High-density development is concentrated around major cities, while large parts of Europe remain very sparsely built up.

The estimation of the effect of extreme precipitation on land development follows three well-established approaches in the literature on climate damages and adaptation: a cross-section (Ricardian) model, a long-difference model, and a first-difference model. The cross-section model compares outcomes across places with different long-run climates, capturing very long-term adjustments, but it is vulnerable to omitted-variable bias (Hsiang, 2016). The model is estimated over a 20-year period (2001-2020), to ensure that weather events are averaged over a sufficiently long period to be interpreted as climate indicators. The long-difference model, following Burke and Emerick (2016), compares changes between the first and last periods in the data. The change in land development, measured as the difference in built-up share between 2020 and 1975, is regressed on the corresponding change in extreme precipitation, defined as the difference between the mean annual extreme precipitation for 2016–2020 and that for 1971–1975. This design captures adaptation over several decades while controlling for all time-invariant cell characteristics. Finally, first-difference panel models, in the spirit of Dell et al. (2012), capture shorter-run responses by

[3] In the climate econometrics literature, *weather* refers to daily precipitation and temperature at a given location, whereas *climate* denotes weather averaged over longer periods of time (Deschênes and Greenstone, 2012). The data used here consist of daily weather observations at the cell level, aggregated over intervals of at least five years. Accordingly, the term *climate* is generally more appropriate, and *weather* is employed only when referring to the original daily observations. While individual floods are triggered by extreme precipitation (i.e. weather events), flood risk is linked to the frequency of extreme precipitation days, which is a climate variable.

[4] Although average built-up shares vary widely across countries, the upward trend is common: in Germany the share increased from 1.5% to over 2.5%, whereas in Russia it rose from 0.14% to 0.25%.

relating changes in built-up share to changes in extreme precipitation from one period to the next. Since land-use data are available only every five years, responses can be observed only at five-year intervals. All specifications include controls for a range of climate variables following Kotz et al. (2022) to ensure that the effect of extreme precipitation is additional to other changes in the climate that could influence land-use decisions (for example via agricultural productivity).

Given the fine spatial scale of the analysis, consistent long-term data on local factors that influence building activity are scarce. Some of these factors may also be shaped by extreme precipitation itself: for example, investments in flood defences, water-retention areas, sewage capacity, or stricter building standards can reduce expected damages and weaken incentives to relocate. An alternative way to address such confounding is to calculate spatial first differences (SFD) (Druckenmiller and Hsiang, 2018; Linsenmeier, 2023). SFD reduce bias by comparing adjacent cells within the same period, removing unobservable common factors—such as topography, institutions, population or economic growth, and common shocks. The effectiveness of SFD depends on granularity (since it eliminates only influences that vary at scales larger than a cell pair) and adaptation within 0.1° cells remains undetected.

For the damage analysis, the focus is on short- and medium-term effects, so it is enough to track changes across five-year periods rather than using long-difference or cross-section comparisons. The estimation is conducted at the regional (NUTS-3) level without spatial first differences, since adjacent pairs cannot be clearly defined outside a raster grid.

The main results can be summarised in five points. First, adaptation appears mainly over longer horizons. In the cross-section, one additional extreme-precipitation day per year is associated with about –0.455 percentage points of built-up share, while in the long-difference model the effect is much smaller (–0.040), and in the first-difference model it is essentially zero. When coefficients are standardised to account for differences in variation of extreme precipitation and built-up share across time scales, cross-section and long-difference estimates become very similar. SFD estimates are more precise than those in levels. In economic terms, the mean number of extreme-precipitation days explains about 15% of the mean built-up share in the cross-section, about 1% in the long-difference model, and virtually nothing in the first-difference model. Overall, these patterns point to a clearer precipitation signal at longer horizons rather than slow adjustment in planning processes. Robustness checks on the long-difference results with SFD confirm that the findings are not driven by modelling

choices. Even in a simple bivariate model without controls or fixed effects, the estimate is similar to the baseline.

Second, adaptation between 1975 and 2020 was concentrated in rapidly growing, already developed areas. In places that were highly built-up in 1975, additional extreme-precipitation days were associated with both less new construction and slower population growth, whereas in more rural areas there was little growth and no discernible effect. This pattern suggests that rapid expansion created scope to adjust development in response to climate risks. By contrast, there was no clear evidence of differences by local income or exposure to river floods.

Third, the costs of spatial adaptation over the same period were limited. Extreme precipitation did not lead to denser population settlement within built-up areas, nor to systematic shifts in construction toward more distant locations. Development was displaced from directly affected cells to nearby ones, but these spillovers were modest and did not alter the broader settlement structure.

Fourth, extreme precipitation caused substantial damages, and losses rose with the extent of built-up land. Over a five-year period, one additional extreme-precipitation day per year increased flood losses by about EUR 14 million per region—equivalent to roughly 0.03% of regional GDP. Losses were larger in more developed regions: each additional 0.1 percentage point of built-up land added about EUR 0.7 million in damages.

Fifth, adaptation offset only a small share of the increase in flood risk caused by growth in built-up area and climate change. By combining estimates in a simple accounting framework, the rise in losses can be decomposed into distinct drivers. Growth in built-up area accounted for nearly half of the increase, more frequent extreme precipitation for about a quarter, while adaptation through locating buildings in lower-risk areas reduced damages by less than 5%.

Related Literature

The empirical literature on climate adaptation addresses a variety of climate risks—such as heatwaves, wildfires, droughts, and floods—and explores different adaptation margins, including air conditioning, migration, and trade networks (Carleton et al., 2024). A central question is how economic agents adjust to long-term climate changes.[5] Alongside well-established approaches (Dell

[5] See, for example, Burke and Emerick (2016): "Because many of the key climatic changes will evolve on a time-scale of decades, the key empirical challenge is in anticipating how economic agents will adjust in light of these longer run changes."

et al., 2012; Burke and Emerick, 2016; Auffhammer, 2018), new empirical methods such as SFD are being developed (Druckenmiller and Hsiang, 2018; Linsenmeier, 2023). This paper compares results across several of these methods, showing that adaptive capacity increases over time.

While the economic impacts of precipitation are often studied jointly with temperature shocks (Dell et al., 2012), a smaller set of studies focuses on extreme rainfall. Kotz et al. (2022) use global weather and regional output data to estimate the effects of various precipitation and temperature indicators, and find that increased frequency of extreme rainfall events reduces output—particularly in high-income countries and in the services and manufacturing sectors. Damania et al. (2020) show that aggregating data to large (national) spatial scales obscures the effects of local weather. Collalti (2024) finds short-term economic effects from flash floods. This paper controls for a similar set of climate indicators to Kotz et al. (2022) and shows that extreme precipitation also affects building activity, especially over the long term.

A strand of the climate literature examines how urban outcomes respond to weather shocks. Using nightlights as a proxy for economic activity and combining data on extreme precipitation and recorded flood events, Kocornik-Mina et al. (2020) show that flooding reduces activity only in recently developed urban areas. Gandhi et al. (2022) follow a similar approach and find that population growth is lower in cities experiencing more floods or extreme precipitation events. These findings suggest that extreme precipitation affects land use—a relationship this paper estimates directly. Magontier and Martinez-Mazza (2024) also examine the impact of extreme rainfall on urbanisation and offer a closely related study to this paper. Using data from Spain, they find that extreme precipitation is associated with an increase in land development, a result they attribute to government payouts to flooded municipalities.

Land use is a classic adaptation margin in agricultural economics (Mendelsohn et al., 1994), where the attention often focuses on allocation of land plots to crops with lower vulnerability to temperature increases (Mendelsohn and Dinar, 2009; Bareille and Chakir, 2023; Wimmer et al., 2024).[6] For instance, Wimmer et al. (2024) document a shift from protein to root crops in response to drought shocks. A more recent urban economics literature has examined how climate risks affect land development, particularly building on greenfield sites. Lin et al. (2024) find increased building

[6]Mendelsohn et al. (1994) half-jokingly suggest that, as temperatures rise, farmland could shift from wheat to corn to grazing, and eventually to retirement villages "to which old folks flock so they can putter around in the warm winters and dry climates." Their broader point is that ignoring adaptation overstates climate damages.

activity in U.S. East Coast areas exposed to coastal flooding. In Castells-Quintana et al. (2021), deteriorating climate conditions are linked to greater urbanization. Hsiao (2023) studies flood risk in Jakarta and the moral hazard created by public flood defences. Ospital (2023) shows that planning restrictions in San Diego push development into wildfire-prone areas. This literature often employs structural urban models to evaluate counterfactual adaptation policies, but climate risks are typically treated as static.[7] Climate finance studies also examine adaptation using asset prices, including real estate, to assess learning from weather shocks. However, these estimates tend to focus on short- to medium-term effects, in part due to the limited availability of long-term, granular housing data (see Giglio et al., 2021).

This paper draws on the climate adaptation literature's focus on long-term adjustments and applies it to a key urban economics outcome: land development. Its main contribution is long-term, large-scale estimates of how building activity adapts to extreme precipitation. The increase in adaptive capacity over time does not seem to be explained by inertia in building processes, but by belief updating. The noise in the climate signal declines with the horizon, which is consistent with ex-ante, belief-driven adaptation (in the sense of Carleton et al. (2024)). The benefits of relocating away from higher-risk areas—in terms of avoided flood damages—increase with the magnitude of changes in extreme precipitation, reflecting the gains from adaptation in the economic-impact framework of Deschênes and Greenstone (2012).

The remainder of the paper is structured as follows. Section 2 describes the datasets and outlines SFD calculations. Section 3 presents stylised facts on built-up area and extreme precipitation in Europe. Section 4 introduces the econometric approaches, and Section 5 reports the main findings. Section 6 introduces a simplified framework to evaluate the reduction in damage due to adaptation. Section 7 concludes with a discussion of policy implications.

[7] For dynamic structural approaches, see Bilal and Rossi-Hansberg (2023).

2 Data

2.1 Data sources

The *Global Human Settlement Layer* project provides information on the built-up environment, derived from Sentinel-2 and Landsat images (Pesaresi and Politis, 2023; Pesaresi et al., 2024). The GHS-BUILT-S dataset captures built-up surface (in square metres) in a spatial raster at 30 arcsec resolution at 5-year intervals over 1975-2020. A building is defined as "any roofed structure erected above ground for any use" and does not include roads, bridges and other infrastructure. The built-up surface is the gross surface bounded by the building wall perimeter ("building footprint"). The GHSL estimation process works backwards from recent to past periods, using satellite images to remove built-up surface step-by-step. As a result, the amount of built-up surface cannot decrease over time. GHS-BUILT-S combines residential and non-residential buildings.[8] The share of the built-up area is calculated by dividing the built-up area by the cell size, after resampling to 0.1 degrees resolution to match E-OBS (see below).[9] Separately, the GHSL Urban Centre Database identifies "urban centres" as contiguous clusters of grid cells with population density 1,500 inhabitants per km^2 and total population 50,000—intuitively, cities of at least 50,000 residents.

E-OBS is a daily gridded meteorological dataset for precipitation and temperature in Europe derived from local weather stations (Haylock et al., 2008). The data are available at 0.1 degree grid resolution from 1950 to present, and has often been used to analyse extreme precipitation, for example in Myhre et al. (2019). [10] Daily precipitation and mean temperature are then used to calculate a number of climate indicators following Kotz et al. (2022). The main indicator for extreme precipitation is the number of days above the 99.9$^{\text{th}}$ percentile of the historical distribution of precipitation over 1961-2020. Additional indicators are the number of days above the 90th percentile, and the total precipitation (in mm) on days above the thresholds. Indicators based on the historical daily precipitation distributions for each cell (as opposed to absolute precipitation

[8] Data for non-residential buildings only are also available on the GHSL website. The data can be downloaded at `https://human-settlement.emergency.copernicus.eu/download.php?ds=bu`

[9] Grid cell size varies with latitude due to the spherical nature of the coordinate reference system (here WGS84). While 0.1 degrees correspond to approximately 11 km in latitude, the distance represented by 0.1 degrees of longitude decreases as you move further from the equator. For example, in Agrigento 0.1 degree longitudes correspond to 8.9km, so that the size of a cell is about 8.9 km^2. In Trondheim, 0.1 degree longitude correspond to 5km and the cell size is about 55km^2.

[10] The data can be downloaded from the Copernicus Data Store (version 30.0e, product type: ensemble mean): `https://cds.climate.copernicus.eu/datasets/insitu-gridded-observations-europe?tab=download`.

thresholds in mm) help account for local climate expectations. The same amount of precipitation in mm will have different consequences in an area that experiences intense precipitation more often. Additional indicators for precipitation are the number of wet days (precipitation above 1mm) and standardised monthly precipitation deviations. [11] Indicators based on daily temperature are the annual mean temperature, and the annual day-to-day temperature variability.[12] All indicators are calculated annually between 1961 and 2020, and then averaged for 5- and 20-year intervals.

Low-elevation plains and areas close to rivers are exposed to flooding in case of extreme precipitation. Elevation (max) and slope (max) are downloaded from *Earthenv*, which provides topographic variables at 1km resolution (Amatulli et al., 2018).[13] River variables are downloaded from *HydroSHEDS* (Lehner and Grill, 2013), and then rasterised to calculate the number of rivers in the total river discharge (the size of the rivers) in each cell.[14] Data from Dottori et al. (2022) are used to identify areas particularly vulnerable to river flooding under extreme precipitation.[15] The dataset provides high-resolution (100 m) river flood hazard maps for most of Europe, generated using hydrological models that simulate inundation along 329,000 km of rivers for six different flood return periods. The analysis focuses on flood depth in a 1-in-100-year river flood scenario, a widely used threshold for defining areas with high river flood risk.

Data on the impacts of hydrological events were obtained from the *Disaster Risk Management Knowledge Center (DRMKC)* Risk Data Hub, managed by the European Commission Joint Research

[11] Standardised monthly precipitation deviations are deviations of monthly precipitation $R_{x,m,y}$ (cell x, month m, year y) from the long-term mean $\overline{R}_{x,m}$, divided by the long-term standard deviation $\sigma_{x,m}$, and weighted by each month's long-term share of annual precipitation $\overline{R}_{x,m}/\overline{RA}_x$:

$$RM_{x,y} = \sum_{m=1}^{12} \frac{R_{x,m,y} - \overline{R}_{x,m}}{\sigma_{x,m}} \frac{\overline{R}_{x,m}}{\overline{RA}_x}.$$

See also Holtermann (2020) for details.

[12] The day-to-day temperature variability is calculated as in Kotz et al. (2022), who in turn refer to Barrios et al. (2010). The indicator captures the mean of the monthly standard deviations of daily temperature $T_{x,d,m,y}$ (cell x, day d, month m, year y) from the monthly average $\overline{T}_{x,m,y}$:

$$\widetilde{T}_{x,y} = \frac{1}{12} \sum_{m=1}^{12} \sqrt{\frac{1}{D_m} \sum_{d=1}^{D_m} (T_{x,d,m,y} - \overline{T}_{x,m,y})^2},$$

where D_m is the number of days in a month.

[13] `https://www.earthenv.org/topography`

[14] `https://www.hydrosheds.org/products/hydrorivers`

[15] `https://jeodpp.jrc.ec.europa.eu/ftp/jrc-opendata/CEMS-EFAS/flood_hazard/`.

Centre (JRC). The database documents severe weather events and natural disasters in Europe since 1980, drawing on records from the Emergency Events Database (EM-DAT), Historical Analysis of Natural Hazards in Europe (HANZE), the Dartmouth Flood Observatory (DFO) Global Active Archive of Large Flood Events, and the Cooperative Open Online Landslide Repository (COOLR). Each record contains information on the event date, duration, and geographic location (available down to the NUTS-3 level), as well as the type of hazard.[16] The impacts of each event are measured in terms of population and economic losses. Hydrological events in the database include floods and related hazards such as landslides. For the purposes of this analysis, all hydrological events recorded at the NUTS-3 level between 1980 and 2020 are aggregated into five-year intervals to facilitate matching with land-use and climate data.

Finally, per capita GDP for 2020 at NUTS-3 region level is taken from *Eurostat / GISCO* (Geographic Information System of the Commission).

2.2 Final datasets

For the main analysis in Sections 5.1-5.4, GHSL and terrain data are resampled to have the same resolution and dimension as E-OBS, i.e. 0.1° resolution, covering only Europe. Resampling sums the built-up area in nearby cells for GHSL data, and averages nearby cells for climate and terrain variables. The built-up share in each cell is then calculated by dividing the built-up area by the cell area. The process is repeated for each year from 1975 to 2020 (at five-year intervals). The data are then spatially first differenced (see Section 2.3). The cross-section dataset uses built-up share for 2020 and 2000-2020 means for climate variables. Long differences are calculated as the difference between built-up share in 2020 and 1975, and extreme precipitation and other climate data as the differences between means for 2015-2020 and 1970-75. First differences are calculated similarly (end-period values for built-up share and period means for climate variables) for all five-year periods between 1975 and 2020. This process results in 3 x 2 datasets: cross-section, long-difference and first-difference data, each in levels and SFD. Appendix A reports summary statistics tables for the datasets in levels. For the damage estimates in Section 5.5 the data are averaged for each NUTS-3

[16] NUTS-3 regions are the smallest territorial units in the European Union's Nomenclature of Territorial Units for Statistics (NUTS) classification, typically corresponding to small administrative districts such as counties, provinces, or major city boroughs.

area, and then matched with DRMKC data (aggregated at five-year intervals, but without SFD or first differences).

2.3 Spatial first differences

Spatial first differences are calculated with the `terra` package by shifting the cell grid by one unit to the right (East), and then taking the difference between the original and the shifted values. This is done for each layer, i.e. each variable and period.

Figure 1 illustrates the effect of spatial first differencing. The top panel displays the distribution of days with precipitation above the 99.9^{th} percentile between 2001 and 2020. The original distribution is right-skewed and approximately normal, with relatively few zero observations. Spatial first differencing re-centres the distribution at zero, increases the number of zero values, and reduces its dispersion. The bottom panel shows the distribution of built-up area in 2020. Before spatial first differencing (Levels, in blue), the distribution is censored at zero—since built-up area cannot be negative—and exhibits a pronounced right tail. After applying spatial first differencing (SFD, in orange), the distribution becomes approximately symmetric and centered around zero. In both cases, there is a large number of observations with no built-up area.

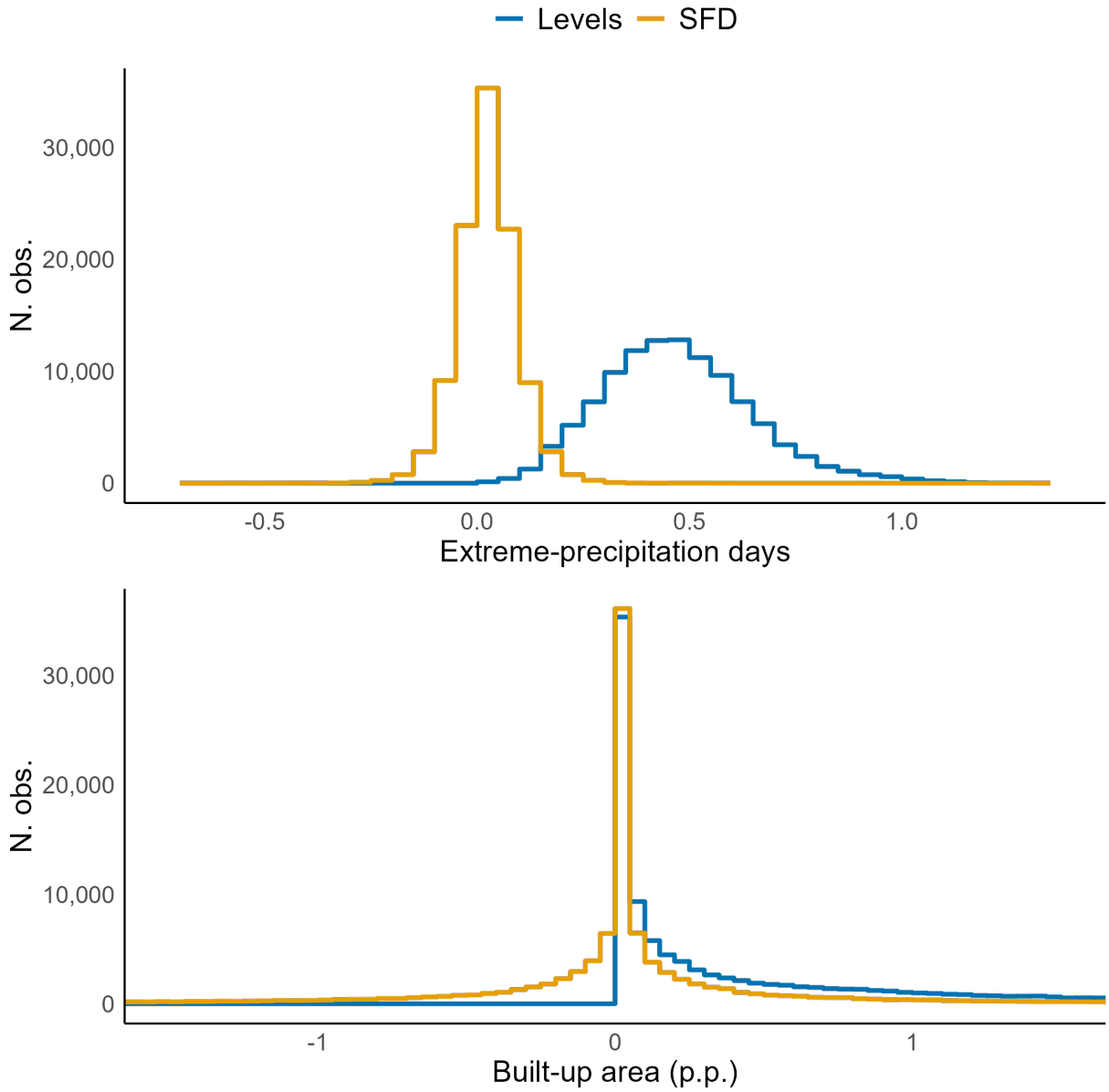

Figure 1: Top: Distribution of days with precipitation above the 99.9th percentile (2001–2020). **Bottom:** Distribution of built-up area (percentage points) in 2020. Comparison is shown for raw data (Levels) and spatial first differences (SFD). The built-up area distribution is truncated at −1.5 and +1.5 percentage points.

3 Built-up area and extreme precipitation in Europe

This section has two objectives. First, it documents four stylised facts about built-up area and extreme precipitation in Europe that frame the subsequent econometric analysis. Second, it explores the empirical association between the two variables and shows how spatial first differences help to

isolate that relationship.[17]

3.1 Stylised facts

1. *Low-density areas predominate, with built-up surface concentrated around urban conglomerations.* The top panel of Figure 2 shows the spatial distribution of built-up area in 2020, highlighting urban centres such as London, Paris, and Madrid. Other dense clusters include the Ruhr region, the Benelux countries, and parts of Northern Italy. In contrast, vast areas across Central, Eastern, and Northern Europe remain very sparsely developed, with most grid cells showing minimal built-up coverage.

2. *Growth in built-up surface between 1975 and 2020 is also concentrated in urban areas.* Average built-up coverage in Europe rose from 0.44% to 0.82% over the period—a relative increase of 86% (0.38 percentage points). The bottom panel of Figure 2 shows that this expansion is almost entirely confined to pre-existing high-density zones, with negligible growth in rural or mountainous regions.

3. *Extreme precipitation varies substantially across regions.* The top panel of Figure 3 shows the 99.9^{th} percentile of daily precipitation at each grid cell over the period 1961–2020. This value serves as a local threshold for identifying extreme-precipitation days. Thresholds tend to be higher in coastal regions—particularly along the Atlantic seaboard—and in mountainous areas such as the Alps and the Pyrenees, reflecting the greater intensity of precipitation events in these environments. Central and Eastern parts of the continent show significantly lower thresholds. This approach captures how unusual an event is by local standards, under the assumption that areas with higher thresholds may be better adapted to handle intense precipitation than those where such events are rarer.

4. *The frequency of extreme-precipitation days has increased across most of Europe.* Between 1971–75 and 2016–20, the average annual count of days above the 99.9^{th}-percentile threshold rose from 0.31 to 0.48—an increase of roughly 55%. The bottom panel of Figure 3 highlights broad swathes of France, Germany, Eastern Europe, Spain and the United Kingdom where

[17] Appendix A contains additional descriptive information, including trends in built-up area and extreme precipitation for selected countries, and summary statistics tables matching the cross-section, long-difference and first-difference models.

extreme events have become more common. Notably, several regions with already high thresholds—such as the Atlantic coast and the Alps—also record substantial gains, pointing to a general intensification of heavy precipitation, while only a few areas register declines.

3.2 Relationship between built-up area and extreme precipitation

The core hypothesis is that greater exposure to extreme precipitation curbs the expansion of built-up surface. Figure 4 offers a first visual inspection. The top panel plots built-up area in 2020 against the average number of extreme-precipitation days during 2001–2020; no systematic association is visible. The bottom panel, based on spatial first differences, uncovers a pronounced negative slope. Cells experiencing larger increases in extreme precipitation tend to record smaller gains (or larger declines) in built-up area. As expected, differencing compresses variance in both variables, yet the downward relationship remains clear. A comparable exercise with long-difference data for 1975–2020 (not shown) yields a similarly negative pattern.

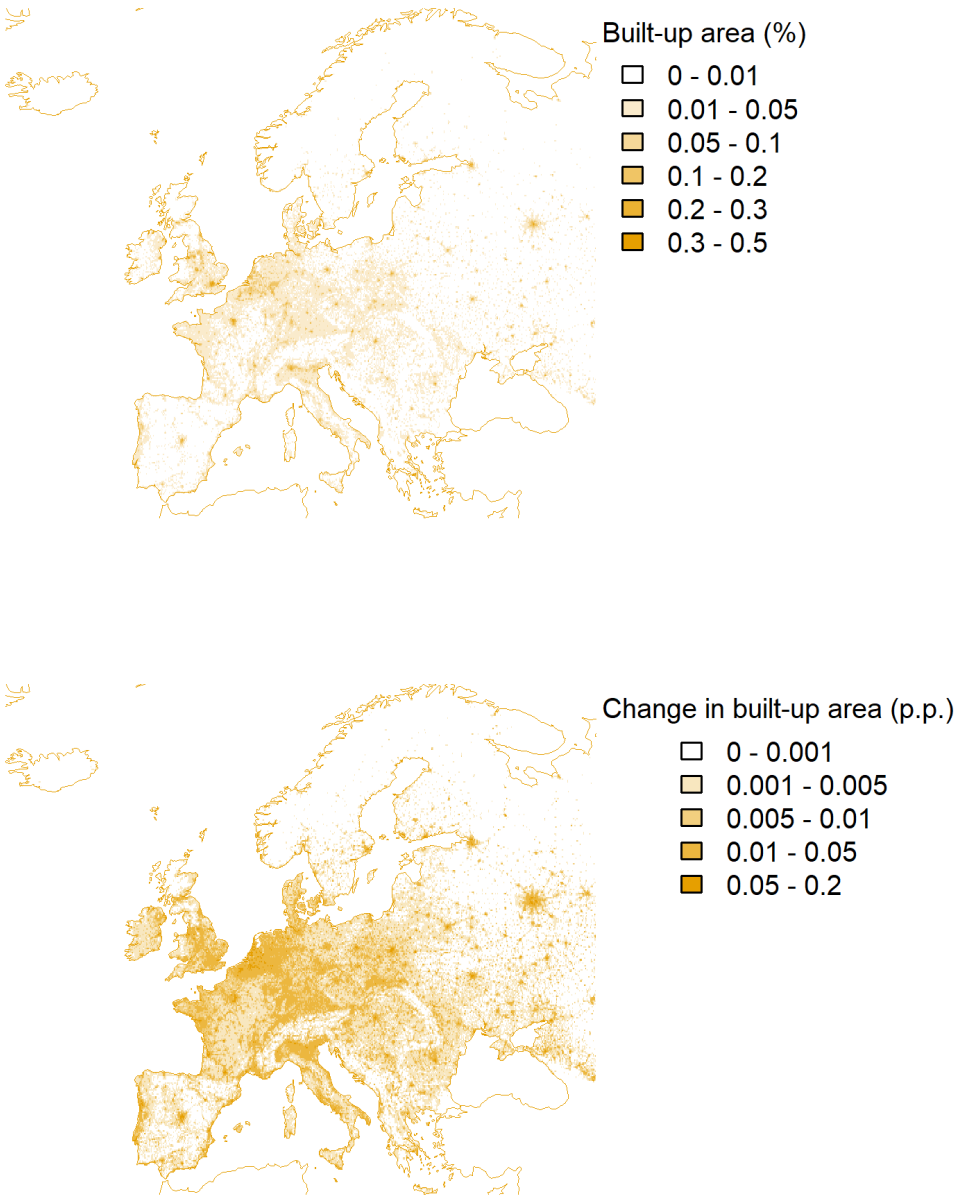

Figure 2: Spatial distribution of built-up area. **Top**: built-up share in 2020 (% cell area). **Bottom**: change in built-up share, 1975–2020 (percentage points).

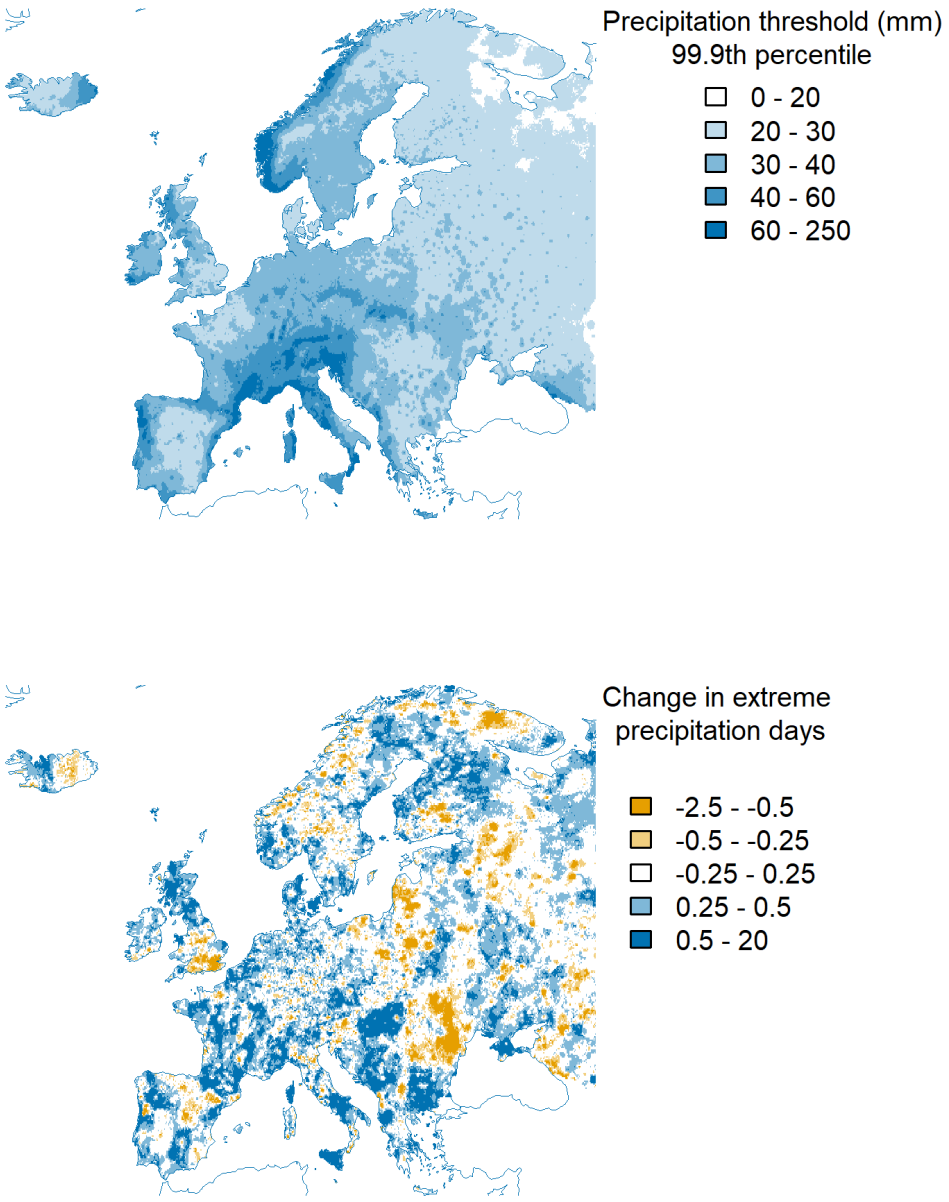

Figure 3: Spatial distribution of extreme precipitation. **Top**: local threshold for an extreme-precipitation day (99.9th percentile of daily precipitation, 1961–2020; mm). **Bottom**: change in the average annual number of extreme-precipitation days, 1971–75 to 2016–20.

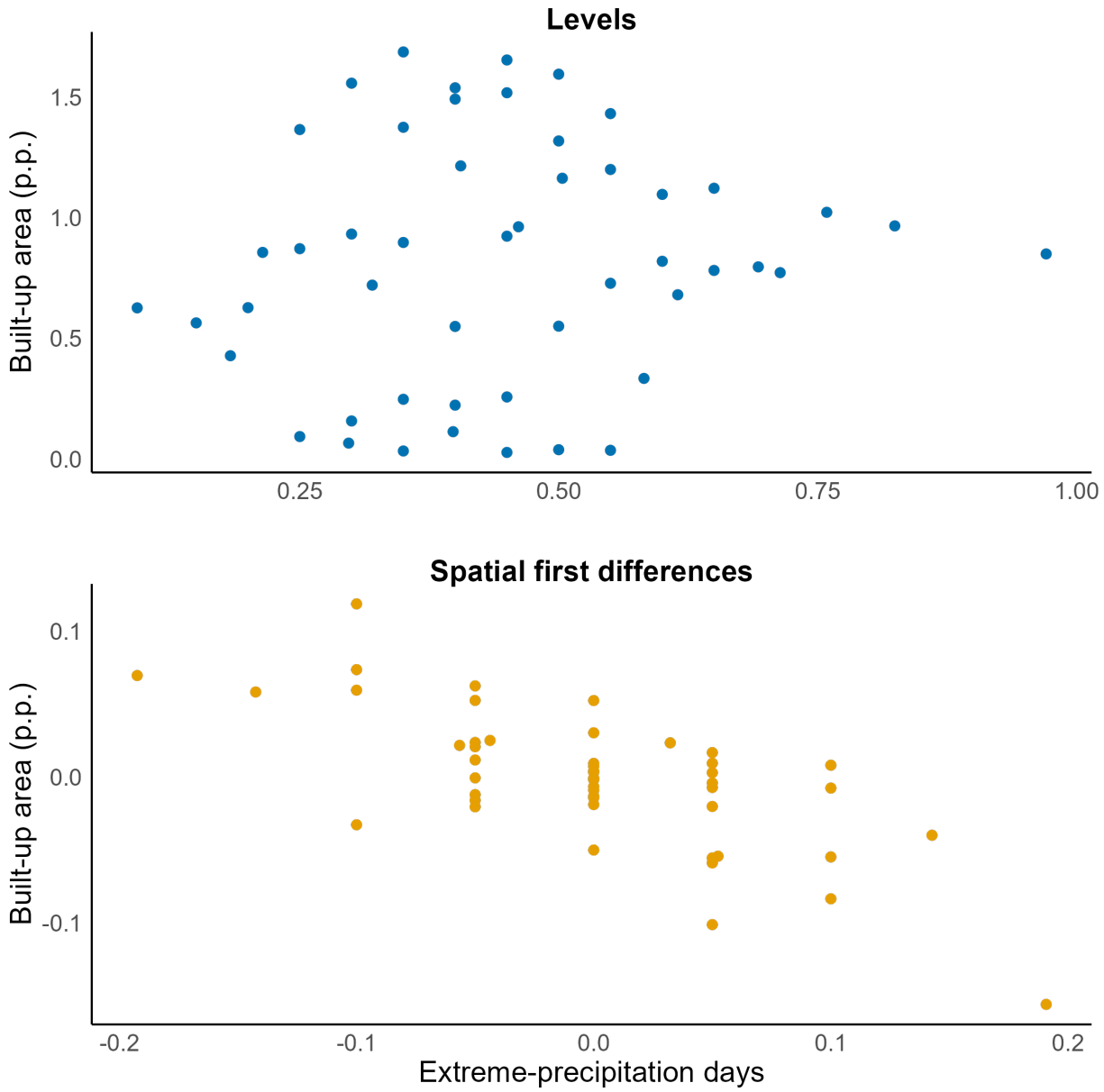

Figure 4: Relationship between extreme precipitation and built-up area from 1975 to 2020. Extreme precipitation is measured as the average number of days per year with precipitation above the 99.9th percentile, and built-up area is expressed as a share of cell area (in percentage points). Observations are aggregated into 50 bins. **Top:** Raw data in levels. **Bottom:** Spatial first-differences applied.

4 Models

Hypotheses

The analysis is guided by three main hypotheses. First, extreme precipitation discourages land development: cells experiencing more frequent extreme precipitation tend to have a lower built-up share. Second, adaptation is gradual, so the negative effect strengthens over longer horizons as weather provides only noisy signals about climate and learning takes time (Kala, 2017). Third, adaptation differs between urban and rural areas, reflecting differences in demand for buildings and land availability. In cities, land scarcity makes it harder to relocate construction, while rapid growth may facilitate adjustments in location patterns.

These hypotheses are tested using three established approaches in the climate damages literature.[18] The cross-sectional (Ricardian) model provides long-run estimates under the assumption of full adaptation, the long-difference model compares development across decades to capture medium-run effects, and the first-difference model identifies short-run responses at five-year intervals. A final, auxiliary validation examines whether extreme precipitation is associated with economic damage. This test is presented at the end of the analysis, since damage data are available only at regional (as opposed to cell) level.

Identification

The core identification issue is to separate long-run climate (that is, expectations about the weather) from short-run weather responses. Longer horizons better capture expectations by averaging over many years, but they increase exposure to omitted-variable bias because other slow-moving determinants of development—such as infrastructure, regulation, migration and economic growth—also evolve over long periods. Shorter horizons reduce this risk but may reflect reactions to weather events even when expectations have not changed.

To mitigate omitted-variable concerns when using long-term data, three tools are applied. First, long differences use changes in development and in exposure to extreme precipitation between distant periods to absorb time-invariant local factors (for example, terrain and persistent settlement patterns). Second, additional climate controls (such as temperature, wet days and variability) account for climate dimensions that are correlated with extreme precipitation and also affect development

[18] See Hsiang (2016); Auffhammer (2018); Kolstad and Moore (2020); Carleton et al. (2024) for reviews of different approaches to estimating climate damages and adaptation.

(e.g. via agricultural output). Third, country fixed effects restrict identification to within-country variation and absorb national shifts in policy, macroeconomic conditions and measurement that are common to all cells.

Even after these precautions, omitted-variable bias may remain. For extreme precipitation, protective measures—such as flood defences, expanded sewage capacity and tighter building standards—reduce expected damages and therefore weaken the incentive to relocate. Investments in emergency response can further limit losses, and ex post disaster aid may even spur rebuilding in affected areas. Ignoring these channels attenuates the expected negative association between extreme precipitation and local built-up area, biasing estimates of spatial adaptation towards zero.

Information on these forms of adaptation is not standardised or consistently available. Spatial first differences (SFD) offer an alternative to control for unobserved variables by differencing values for adjacent cells. SFD thereby remove factors that are common to the pair—such as topography, institutions and common shocks. Only the remaining variation after SFD is used for estimation (Druckenmiller and Hsiang, 2018; Linsenmeier, 2023). Applying SFD to the climate regressors means that identification comes from very local differences in long-run exposure to extreme-precipitation days.[19]

i. Cross-section model

Time is not explicit in the cross-section model, but the assumption is that agents have optimised their choices according to the local climate, and the results are interpreted in terms of long-run equilibrium adaptation. Locations with more frequent extreme precipitation events are used as a counterfactual for the response of locations with less frequent extreme events (Mendelsohn et al., 1994; Auffhammer, 2018). The following cross-section model is estimated:

$$y_{i,k} = \rho_{cs} R_{99.9,i} + C_i' \beta_{cs} + X_i' \gamma + \delta_k + \varepsilon_i \tag{1}$$

where $y_{i,k}$ is the built-up share of cell i in country k at the end of the period (in 2020). $R_{99.9,i}$ is the average annual number of days with precipitation above the 99.9$^{\text{th}}$ percentile of the distribution for cell i during the period 2001-2020. C_i denotes a vector of climate variables capturing means and deviations for temperature and precipitation, including mean annual precipitation, standardised

[19]The effectiveness of SFD depends on data granularity: it purges influences that vary at scales larger than a cell pair.

monthly precipitation deviations, number of wet days, mean annual temperature (and its one-period lag), day-to-day temperature variability, the first difference of the temperature mean, and the interaction of the temperature mean with its first difference.[20] X_i is a vector of cell characteristics, including terrain (elevation, slope and roughness) and hydrological (number of rivers, total river discharge) variables. δ_k are country fixed effects that capture the average share of built-up area for cells in country k. The main coefficient of interest is ρ_{cs}, which captures the effect of one additional day of extreme precipitation (annual average) on the built-up share.

The SFD version of the cross-section model is

$$\Delta^s y_{i,k} = \rho_{cs}\, \Delta^s R_{99.9,i} + (\Delta^s C_i)'\beta_{cs} + (\Delta^s X_i)'\gamma + \delta_k + \varepsilon_i. \tag{2}$$

Here the superscript s in Δ^s denotes a spatial first difference, comparing two points in space rather than two moments in time. For example, taking the built-up share of adjacent cells i and $i+1$, the spatial first difference is defined as $\Delta^s y_i = y_i - y_{i+1}$, where $i+1$ is the cell immediately to the right (east) of i. By the same logic, $\Delta^s C_i$ and $\Delta^s X_i$ are the spatial first-difference vectors of climate and other cell characteristics, respectively. The term $+\delta_k$ captures common country-level factors that may influence comparisons across cell pairs, such as regional or national planning processes.

ii. Long-difference model

The long-difference (LD) model explains the change in built-up surface in terms of the change in average weather conditions, taking two periods far apart. Identification is based on differential climate trends, rather than different climates (Burke and Emerick, 2016). Differencing controls for all factors that remain constant over time, e.g. existing flood-protection infrastructure. The two periods used for differencing are far apart to leverage long-term variation in climate, rather than shorter-term weather shocks. In the context of this study, a long interval also allows time to adjust long-term planning and building processes [21]

The LD model compares the change in land use with the change in climate for two 5-year periods, 1975-1980 and 2015-2020. The variables are the same as in the cross-section model, but expressed as differences between these two periods. Cell characteristics that do not change, such as terrain and

[20] See Kotz et al. (2022) and Section 2 for details.

[21] Time to develop residential properties is about three years (Oh et al., 2024), but urban planning can have longer horizons. Jackson (2016) documents a large increase in land use regulations in California in the 1980s and 1990s.

hydrology, drop off the model. The resulting LD model is

$$\Delta y_{i,k} = \rho_{ld} \Delta R_{99.9,i} + (\Delta C_i)' \beta_{ld} + \delta_k + \varepsilon_i, \tag{3}$$

where $\Delta y_{i,k} = y_{i,k,2020} - y_{i,k,1975}$ is the change in the share of built-up area between 1975 and 2020, and $\Delta R_{99.9,i} = R_{99.9,2015:2020,i} - R_{99.9,1975:1980,i}$ is the change in the average number of extreme precipitation days between the first period (1975-1980) and the second period (2015-2020). Similarly for all other climate variables in ΔC_i. δ_k are country fixed effects that capture the average change in the share of the built-up area for cells in country k. Equation (3) can also be estimated with SFD. The dependent variable is the spatiallyfirst-differenced building activity between 1975 and 2020, and the climate variables represent the spatially first-differenced change in climate.

iii. First-difference model

Shorter-term adaptation is estimated with a first-difference panel model, comparing changes in land use with changes in climate over successive 5-year periods between 1975 and 2020. Here, first-difference is temporal rather than spatial, and the change in built-up share between two periods reflects new building activity.[22] The specification is analogous to the LD model in Equation (3), but differences are taken between adjacent periods $t + 1$ and t. For example, $\Delta y_{i,k,2020} = y_{i,k,2020} - y_{i,k,2015}$ is the change in built-up share from 2015 to 2020, while $\Delta R_{99.9,i,t} = R_{99.9,2015:2020,i} - R_{99.9,2010:2015,i}$ is the change in extreme precipitation days between the two adjacent 5-year intervals. The resulting first-difference model is

$$\Delta y_{i,k,t} = \rho_{fd} \Delta R_{99.9,i,t} + (\Delta C_{i,t})' \beta_{fd} + \delta_k + \eta_t + \varepsilon_{i,t}, \tag{4}$$

where δ_k are country fixed effects that capture the average change in the share of the built-up area for cells in country k over all five-year intervals, and η_t are period fixed effects. Equation (4) can also be estimated with SFD, in which case differences are taken both over space and over time.

Extensions and robustness of the SFD long-difference baseline

The SFD long-difference specification is selected as the baseline for robustness checks and further analysis. This model provides long-term estimates for a specified period, and the combination of temporal and spatial differencing offers a conservative strategy against omitted variable bias.

[22] Differencing also ensures stationarity of the dependent variable, since built-up share increases over time.

The baseline uses longitudinal spatial first differences (adjacent east–west cells), measures extreme precipitation as the mean annual number of days above the cell-specific 99.9^{th} percentile, and reports Conley standard errors with a 100 km cut-off. Building on this baseline, the following analyses are conducted:

- *Robustness:* switch to latitudinal SFD (north–south); use alternative definitions of extreme precipitation; trim outliers; cluster standard errors at the country level; estimate separate models for positive versus negative changes in extreme-precipitation days; exclude cells with no buildings in 1975; bivariate model without covariates or fixed effects.
- *Timing of adaptation:* re-estimate the baseline LD SFD specification over intervals that all start in 1975 and end in five-year steps from 1980 to 2020.
- *Neighbourhood effects:* include six queen–contiguity spatial lags (neighbours that share an edge or a corner) of extreme precipitation to capture spillovers from neighbouring cells.
- *Initial urbanisation:* compare effects across areas by quartiles of the built-up share in 1975.
- *Risk and income heterogeneity:* report long-difference coefficients and built-up growth rates by quartile of flood risk—proxied by modelled flood depth in a 1-in-100-year event—and by quartile of 2020 per capita income.

Damages

In the models above, the maintained assumption is that extreme precipitation is associated with economic damage, which in turn discourages local development. To assess this mechanism, data from the DRMKC at the NUTS-3 level are used to measure economic damage from major hydrological disasters (primarily floods), together with climate variables spatially aggregated to the same level.

Large hydrological disasters are rare at the NUTS-3 level, making long-difference estimation impractical without very long averaging windows. Instead, a fixed-effects panel model is estimated at five-year intervals, for consistency with the rest of the study. The focus is therefore on climate-scale relationships rather than links between individual extreme-weather events and damage. Spatial first differencing is not applied because NUTS-3 regions do not form a regular grid, making the definition of adjacent pairs ambiguous.

The following fixed-effects panel model is estimated:

$$y_{r,t} = \phi\, R_{99.9,r,t} + C'_{r,t}\beta + \mu_r + \eta_t + \varepsilon_{r,t}, \tag{5}$$

where r indexes NUTS-3 regions and t denotes the five-year window ending in year t. The outcome $y_{r,t}$ is estimated in separate regressions as: (i) the number of disaster events; (ii) total economic damage (EUR); and (iii) economic damage per percentage point of built-up area, each measured over period t. $R_{99.9,r,t}$ and $C_{r,t}$ are defined as in the previous models. μ_r are NUTS-3 fixed effects, η_t are period fixed effects, and $\varepsilon_{r,t}$ is an error term.

5 Results

5.1 Model comparison

To compare the models, results are presented in three steps: raw coefficients, standardised coefficients, and economic magnitudes.

Raw coefficients

Table 1 presents results for three models (cross-section, long-difference, and first-difference) in both levels and spatial first-difference (SFD) form. All models are estimated with Conley standard errors using a 100km cut-off. For brevity, the table reports only the coefficient for the average annual number of extreme precipitation days, defined as days with precipitation above the 99.9$^{\text{th}}$ percentile of a cell's daily precipitation distribution. The table also reports the mean of the dependent variable. Full results, including coefficients for all climate and terrain controls, are provided in Appendix B.

The cross-section model in Equation (1) uses data on the built-up share for 2020 and annual averages of climate variables for 2000–2020. It includes country fixed effects and controls for terrain characteristics. In the levels specification, reported in column (1) of Table 1, one additional day (annual average) with precipitation above the 99.9$^{\text{th}}$ percentile lowers the built-up share of a cell by 0.455 percentage points. The coefficient is comparable in the SFD specification in column (2) (-0.446), but its standard error is smaller. Both estimates are statistically significant at the 1% level.

The long-difference model in Equation (3) relates the change in the built-up share from 1975 to 2020 to the change in extreme precipitation between 1970–1975 and 2015–2020. Terrain controls

are eliminated by differencing, and country fixed effects absorb mean changes rather than mean levels. The coefficients for the specification in levels (column 3) of Table 1 and SFD (column 4) are -0.061 and -0.040, respectively—an order of magnitude smaller than in the cross-section model. Both coefficients are statistically significant, and standard errors are smaller in the SFD model. Focusing on the SFD model in column (4), a one-day increase in the annual average number of extreme precipitation days between 1970–1975 and 2015–2020 reduces the built-up share by 0.040 percentage points.

The first-difference model in Equation (4) relates changes in the built-up share to changes in extreme precipitation across all five-year intervals from 1975 to 2020. In the levels specification (column 5 of Table 1), the coefficient for the average number of extreme precipitation days is positive (0.0005) and not significant. In the SFD model (column 6), the coefficient turns negative and significant (-0.0007).

Table 1: Comparison of cross-sectional, long-difference and first-difference models

	Cross-section		**Long-difference**		**First-difference**	
	Levels	SFD	Levels	SFD	Levels	SFD
	(1)	(2)	(3)	(4)	(5)	(6)
Extreme rainfall days	-0.455***	-0.446***				
	(0.153)	(0.084)				
Δ Extreme rainfall days			-0.061**	-0.040***	0.0005	-0.0007***
			(0.025)	(0.012)	(0.0006)	(0.0002)
Climate controls	Yes	Yes	Yes	Yes	Yes	Yes
Terrain controls	Yes	Yes				
Country fixed effects	Yes	Yes	Yes	Yes	Yes	Yes
Year fixed effects					Yes	Yes
R^2	0.25297	0.07344	0.26887	0.00667	0.19933	0.00094
Observations	108,070	106,668	108,070	106,668	849,573	806,769
Dependent variable	Built-up	Built-up	Δ Built-up	Δ Built-up	Δ Built-up	Δ Built-up
Mean Dependent	0.818	-0.0006	0.380	-0.0006	0.048	-0.0001

Conley (100km) standard-errors in parentheses
*Signif. Codes: ***: 0.01, **: 0.05, *: 0.1*

Notes: The dependent variable is built-up area for the cross-sectional model, and the change in built-up area for the long-difference and first-difference models. Extreme rainfall days defined as days with rainfall above the 99.9th percentile.

Standardised coefficients

The results in Table 1 report the effect of one additional extreme precipitation day (annual average) on built-up share. The three specifications exploit different sources of variation. The cross-section model captures wide dispersion in built-up shares but only limited cross-country variation in extreme precipitation. By contrast, the long- and first-difference models harness substantial temporal variation in precipitation but far less variation in built-up shares, particularly in the first-difference specification. To place these estimates on a common scale, Figure 5 plots standardised coefficients with confidence intervals. Standardisation rescales the coefficients by the within-group (after removing fixed effects) standard deviations of both the explanatory and outcome variables, ensuring comparability across specifications that rely on different sources of variation.[23]

Standardised coefficients for the cross-section and long-difference specifications are broadly comparable. In levels, both models indicate that a one-standard-deviation increase in the annual number of extreme precipitation days reduces the built-up share by about 0.04 standard deviations. By contrast, the standardised coefficient in the first-difference model is an order of magnitude smaller and statistically insignificant at the 5% level. In the spatial first-difference (SFD) versions, effects are attenuated but follow the same pattern: a one-standard-deviation increase in extreme precipitation reduces the built-up share by 0.023 standard deviations in the cross-section SFD model, 0.016 in the long-difference SFD model, and only 0.002 in the SFD first-difference model.

[23] Standardised coefficients are defined as

$$\rho^{*} = \hat{\rho}\,\frac{\sigma_R}{\sigma_y},$$

where $\hat{\rho}$ is the raw coefficient and σ_R, σ_y are the within-group standard deviations of precipitation and built-up share. In cross-section (CS) and long-difference (LD) models, within-variation is defined relative to country means. In first-difference (FD), year dummies are also removed. Estimated within-group standard deviations: $\sigma^{y}_{CS} = 1.81$, $\sigma^{y}_{LD} = 0.70$, $\sigma^{y}_{FD} = 0.09$; $\sigma^{R}_{CS} = 0.15$, $\sigma^{R}_{LD} = \sigma^{R}_{FD} = 0.43$. These standard deviations are based on the specifications in levels and are not re-estimated for the SFD models, because most of the variation is mechanically removed by taking differences between adjacent cells.

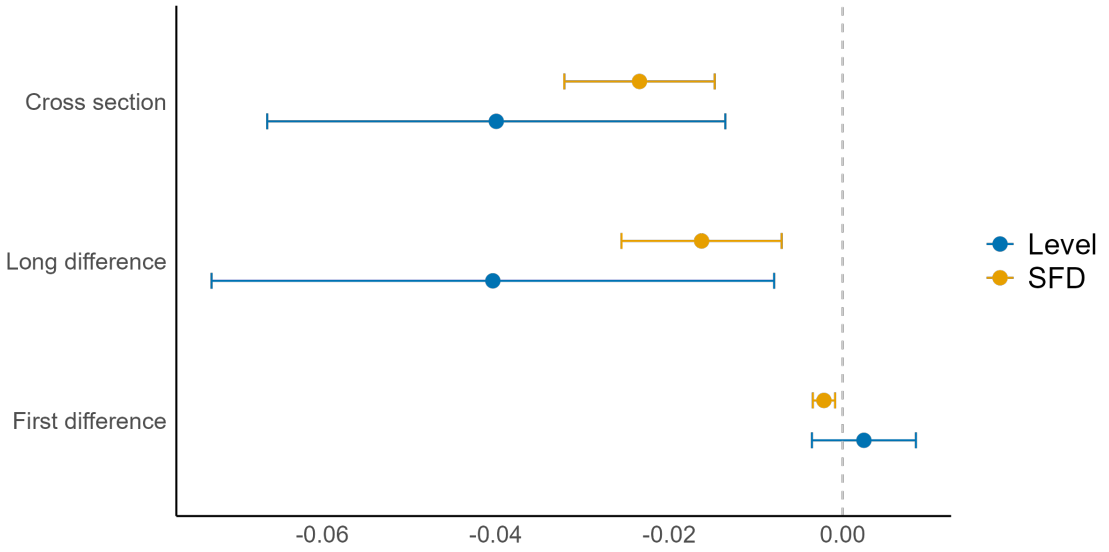

Figure 5: Comparison of standardised coefficients with 95% confidence intervals for cross-section, long-difference and first-difference models (levels and SFD).

Economic magnitudes

Standardised coefficients facilitate comparisons across models that exploit different sources of variation, but they are not easily translated into economic terms. A rough measure of economic impact can be obtained by calculating how much of the mean built-up share is attributable to the mean number of extreme-precipitation days in each specification. This measure is denoted by κ and referred to as the normalised economic effect: the share of the mean built-up area explained by the mean level of extreme precipitation.

Formally,

$$\kappa = \frac{\hat{\rho} \times \mu_R}{\mu_y} = \rho^* \times \frac{\sigma_y/\mu_y}{\sigma_R/\mu_R} \tag{6}$$

where $\hat{\rho}$ and ρ^* are, respectively, the estimated and standardised coefficient on the number of extreme days from each model (using SFD estimates, which are more precise), while μ_y and μ_R are the means of built-up area and extreme precipitation days on the raw (level) data; σ_y and σ_R are the within-group standard deviations. The coefficient of variation of built-up area, $CV_y = \sigma_y/\mu_y$, expresses the relative dispersion of built-up area (similarly for R). The coefficients of variation link standard deviations to means, indicating how large a one-standard-deviation change is relative to the average level. A smaller CV implies that a single standard deviation conveys a stronger signal,

so standardised effects translate into larger magnitudes in relation to the mean. For comparability across models, κ is reported using the SFD estimates, which are more precise.

Table 2 reports the normalised economic effect (κ). The cross-section estimate is the largest, $\kappa_{CS} \approx -14.6\%$, indicating that the mean extreme-precipitation level is associated with a reduction of roughly 14.6% in the mean built-up share. The long-difference effect is much smaller, $\kappa_{LD} \approx -1.1\%$, and the first-difference estimate is essentially negligible, $\kappa_{FD} \approx -0.02\%$.

Table 2 also reports standardised coefficients (discussed above) and coefficients of variation. For built-up share, coefficients of variation are similar in the long- and first-difference models (1.74 and 1.83, respectively) and somewhat larger in the cross-section (2.07), suggesting broadly similar proportional variability at medium and shorter horizons, with additional dispersion only at the very long-term scale. If inertia in building and planning were important, the coefficients of variation would be smaller at shorter horizons than at longer ones; instead, they are of similar magnitude in the first- and long-difference models and only slightly larger in the cross-section, indicating little evidence of inertia.

For extreme precipitation, coefficients of variation fall sharply as the time horizon lengthens: 22.37 in the first-difference model, 2.58 in the long-difference model, and 0.33 in the cross-section. This decline implies that a one-standard-deviation change in precipitation is a much stronger signal in the very long run, helping to explain why, despite similar standardised coefficients, the normalised economic effect is much larger in the cross-section than in the long-difference model.

Taken together, these patterns indicate that differences in κ are driven less by changes in estimated slopes than by the relative dispersion of precipitation across horizons.

Table 2: Estimated standardised economic magnitudes (κ) and coefficients of variation for built-up area (y) and extreme precipitation days (R).

	ρ^*	σ_y/μ_y	σ_R/μ_R	κ (%)
Cross section	-0.023	2.067	0.333	-14.552
Long difference	-0.016	1.738	2.581	-1.094
First difference	-0.002	1.825	22.369	-0.017

Notes: ρ^* denotes the standardised coefficient of built-up area on extreme precipitation days for each specification. σ_y/μ_y and σ_R/μ_R are the coefficients of variation for built-up share and extreme precipitation days, respectively. κ is the standardized economic magnitude expressed as a percentage, calculated as $\kappa = \rho^* \times (\sigma_y/\mu_y)/(\sigma_R/\mu_R)$.

To summarise, the comparisons show: (i) cross-section estimates are larger than long-difference estimates, while first-difference estimates are close to zero; (ii) standardised slopes are broadly similar for cross-section and long-difference; and (iii) the economic effect is larger in the cross-section mainly because precipitation varies less relative to its mean over long horizons, so a one-standard-deviation change represents a larger fraction of the average level and yields a bigger share-of-mean effect. This pattern is consistent with adaptation responding to a clearer precipitation signal at longer horizons, rather than to planning inertia.

Adaptation over time

The model comparison above suggests that adaptation strengthens over longer horizons, as the effect of extreme precipitation on built-up area is larger in long-run than in short-run specifications. To test this more directly, Figure 6 reports forward long-difference estimates from 1975 to successive endpoints between 1980 and 2020. For each endpoint T, the figure reports the coefficient from a regression of built-up share growth, $\Delta y_{i,1975\to T}$, on the change in the number of extreme-precipitation days, $\Delta R_{99.9,i,1975\to T}$, following the long-difference specification in Equation 3 with SFD. Terrain controls are eliminated by differencing, country fixed effects are included, and standard errors are computed using Conley (100km cut-off).

The estimated effect turns negative in the 1990–1995 interval and becomes statistically distinguishable from zero from 2000 onward, with magnitudes that become increasingly negative as T approaches 2020. This pattern is consistent with adaptation effects that accumulate over longer horizons and with a clearer precipitation signal at longer horizons.

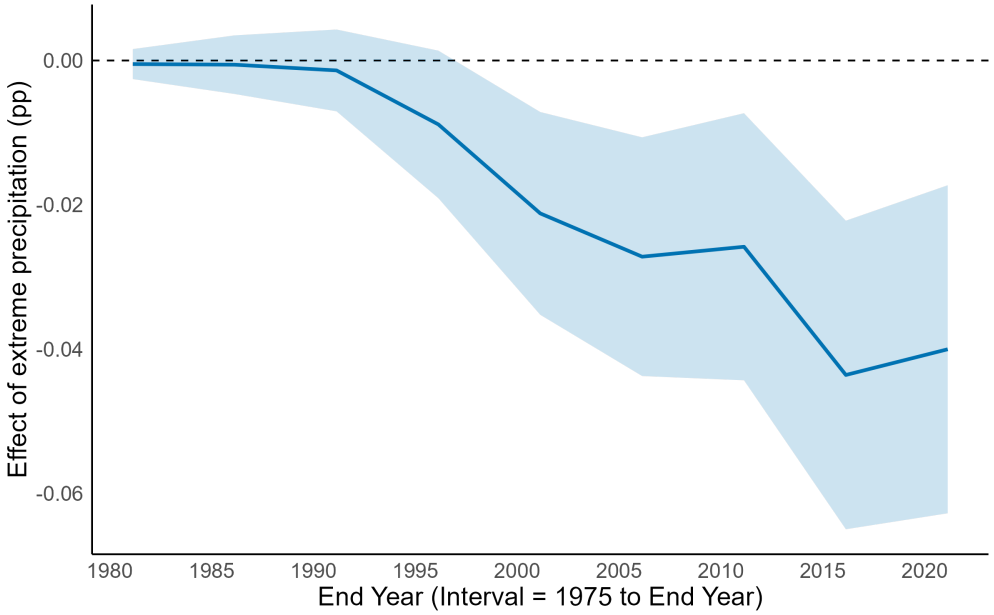

Figure 6: Long-difference models estimated for all intervals from 1975 to 2020. Coefficients for the effect on built-up area of extreme-precipitation days (above the 99.9th percentile). Start year is always 1975, end year increases in five-year steps until 2020. Uses spatial first-differences.

5.2 Robustness

The baseline long-difference model employs longitudinal spatial SFD, measures extreme precipitation as the number of days above the 99.9th percentile, and applies Conley standard errors with a 100 km cut-off. Figure 7 reports the *Baseline* estimate (–0.04 p.p., highlighted in orange) followed by a sequence of robustness checks. *Lat. SFD* replaces the longitudinal SFD with a latitudinal version, where differencing adjacent cells north–south yields a larger coefficient (–0.06 p.p.), possibly reflecting residual omitted-variable bias or stronger adaptation along that axis. *Days ≥ 99.0 pct* uses a 99.0th-percentile threshold, reducing the effect to –0.03 p.p., while *Rain tot. (10 mm)* uses the total precipitation on ≥99.9th-percentile days, rescaled to 10 mm units, yielding –0.01 p.p. *Country S.E. clusters* reports results with standard errors clustered at the country level, producing –0.04 p.p. and narrower confidence intervals, confirming that Conley (100 km) remains the more conservative choice. *Increases* and *Decreases* split the sample by positive and negative changes in extreme-precipitation days; the coefficients are similar, suggesting fairly symmetric effects. *No outliers* trims both the dependent and independent variables at the 1st and 99th percentiles, attenuating the coefficient to –0.02 p.p.. *Built in 1975* restricts the sample to grid cells with strictly positive

built-up area in 1975, yielding –0.04 p.p., consistent in sign and magnitude with the baseline. Finally, *Bivariate* estimates a simple OLS with no climate controls and no fixed effects. The coefficient is similar in magnitude but slightly larger than the baseline (–0.05 p.p.), suggesting that SFD captures most of the confounding influence of other climate variables and country characteristics. All estimates are significant at the 5% level, confirming the robustness of the SFD long-differences specification to key modelling choices.

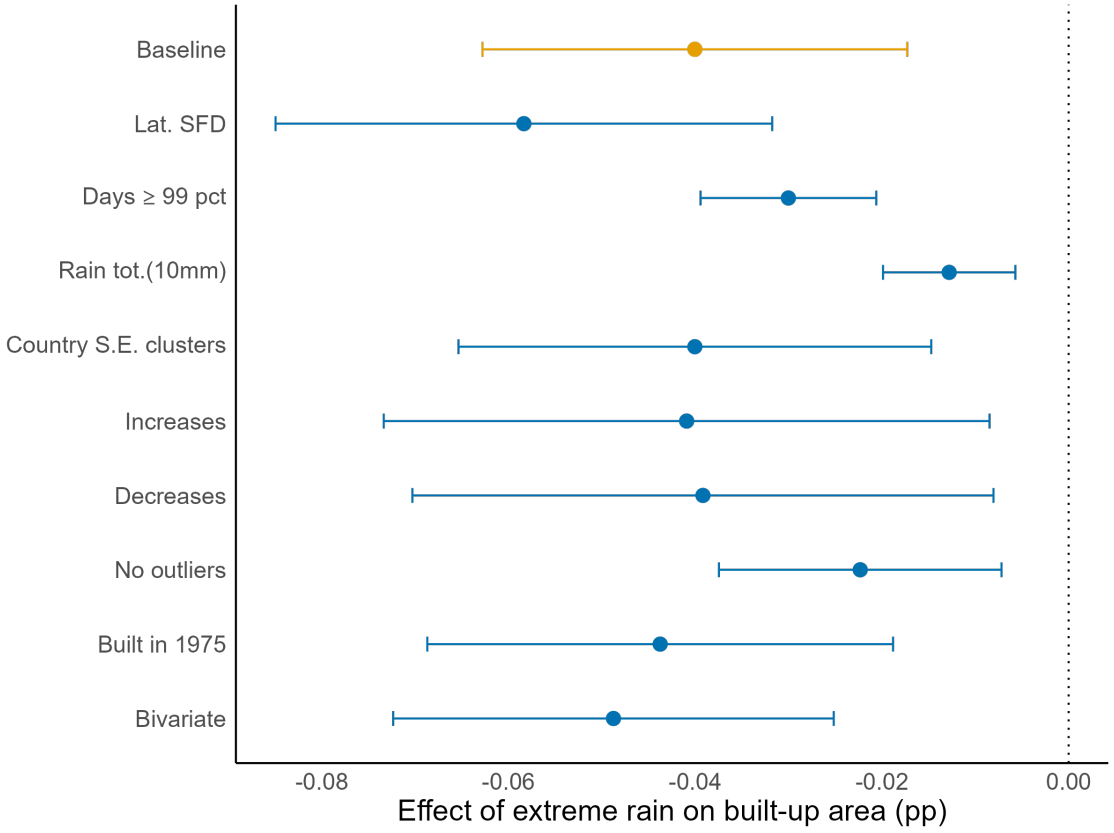

Figure 7: Robustness checks of the long-difference model in its SFD specification (coefficient estimates with 95% CIs). *Baseline* refers to the long-difference specification with longitudinal SFD used in Table 1. *Lat. SFD* denotes latitudinal spatial first differencing. *Days ≥ 99.0 pct* is the number of days with precipitation above the 99.0th percentile. *Rain tot. (10mm)* is total precipitation on days above the 99.9th percentile, expressed in 10 mm units. *Country S.E. clusters* indicates standard errors clustered at the country level. *Increases* and *Decreases* use only observations with positive and negative changes in the number of extreme-precipitation days (days above the 99.9th percentile). *No outliers* trims the distributions for built-up area and extreme precipitation at the 1st and 99th percentiles. *Built in 1975* restricts the sample to grid cells with strictly positive built-up area in 1975. *Bivariate* estimates a simple OLS with no climate controls and no fixed effects.

5.3 Mechanisms

This section examines three mechanisms that may amplify how extreme precipitation affects adaptation. First, land availability: limiting built-up area is more costly where population density is high or land demand from population growth is strong, so responses may differ between urban and rural areas. Second, exposure to risk: the costs of extreme precipitation are likely to be greater in areas more prone to flooding. Third, income: regions with higher incomes may have more resources to invest in adaptation.

Urban versus rural adaptation

Land use dynamics differ markedly between densely built-up urban areas and less developed rural regions. In principle, reallocating development away from high-risk zones should be easier in areas with fewer pre-existing constraints. Figures 8 and 9 test this hypothesis by plotting the effects of extreme precipitation on built-up area and population growth, respectively, across areas with differing initial urbanization. Urbanization is proxied by the share of built-up area in 1975, the first year for which satellite-based land use data are available.

Figure 8 examines heterogeneity in land-use adaptation by grouping cells into quartiles based on their 1975 built-up share.[24] The *top panel* shows built-up area growth (in percentage points) from 1975 to 2020. Growth is highly concentrated in more urbanized areas: the top quartile gained 1.4 p.p. on average, while the bottom quartile saw virtually no change. The *bottom panel* presents marginal effects from a long-difference regression with spatial fixed effects and interactions between quartiles and extreme precipitation (defined as annual precipitation above the 99.9^{th} percentile). These results reveal increasing sensitivity to extreme precipitation with urbanization: an additional extreme-precipitation day reduces built-up growth by 0.051 p.p. in the third quartile and by 0.076 p.p. in the top quartile. In relative terms, the latter implies a 5.4% reduction in new development (0.076 p.p./1.4 p.p.).

Figure 9 repeats the analysis for population. Quartile assignment remains based on 1975 built-up shares. The results are even more pronounced. Only the top quartile experienced positive population growth—an average increase of 2,471 inhabitants, while the other three quartiles saw net declines. The effect of extreme precipitation is statistically significant only in the top quartile: one additional

[24] Cutoff points for the 25th, 50th, and 75th percentiles of the 1975 built-up share are 0.024, 0.15, and 0.49 percentage points, respectively.

extreme-precipitation day per year reduces population growth by 1,113 people, equivalent to 45% of the average increase.

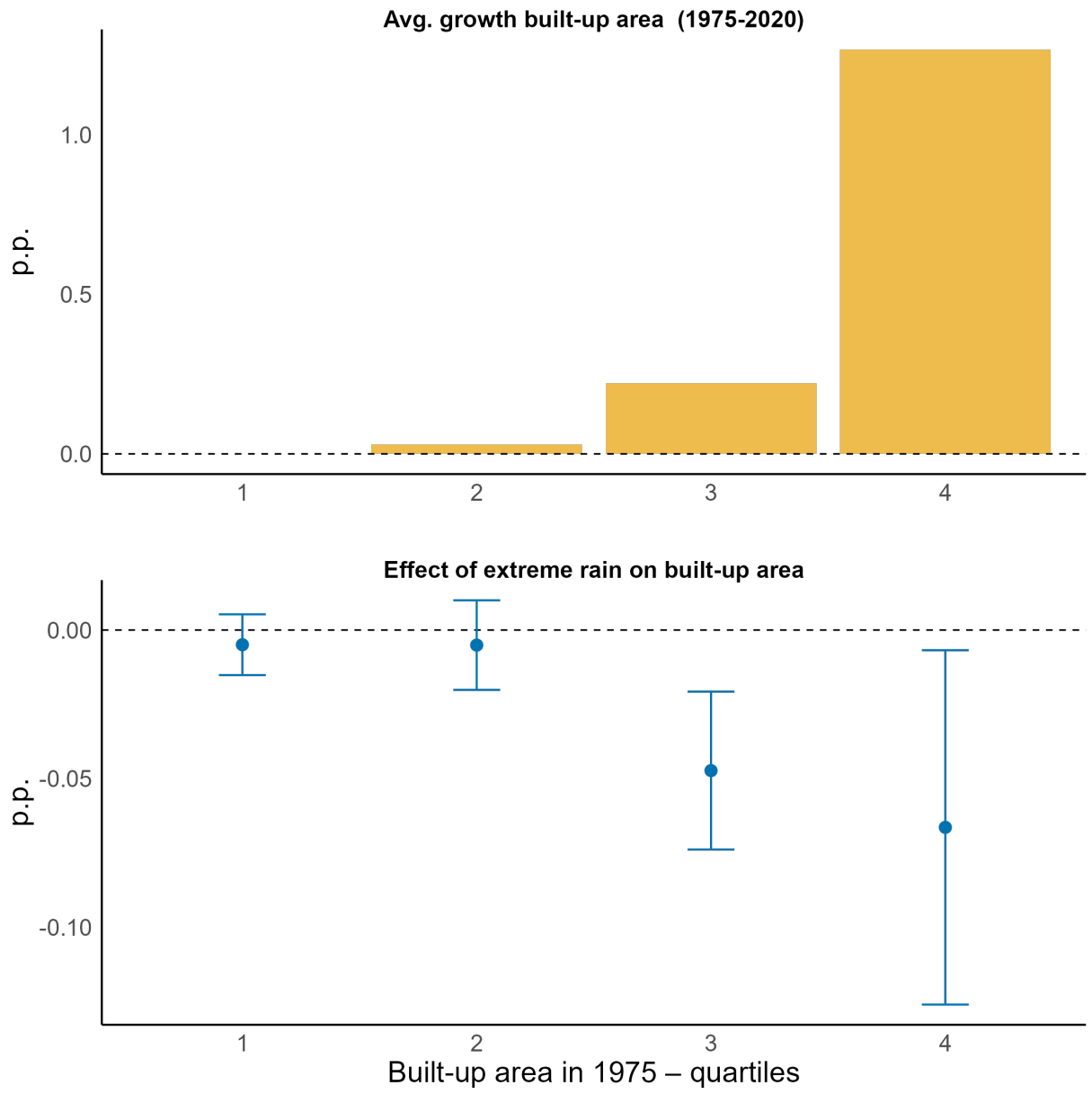

Figure 8: Top: change in built-up area between 1975 and 2020, by quartile of built-up area in 1975. **Bottom**: effect of extreme precipitation (1 additional day above 99.9th percentile) on built-up area, by quartile for built-up area in 1975. Effects are estimated by adding interaction terms to the SFD version of the long-difference model in Equation (3), with added interaction terms for quartile of built-up area. Bands indicate 95% confidence intervals.

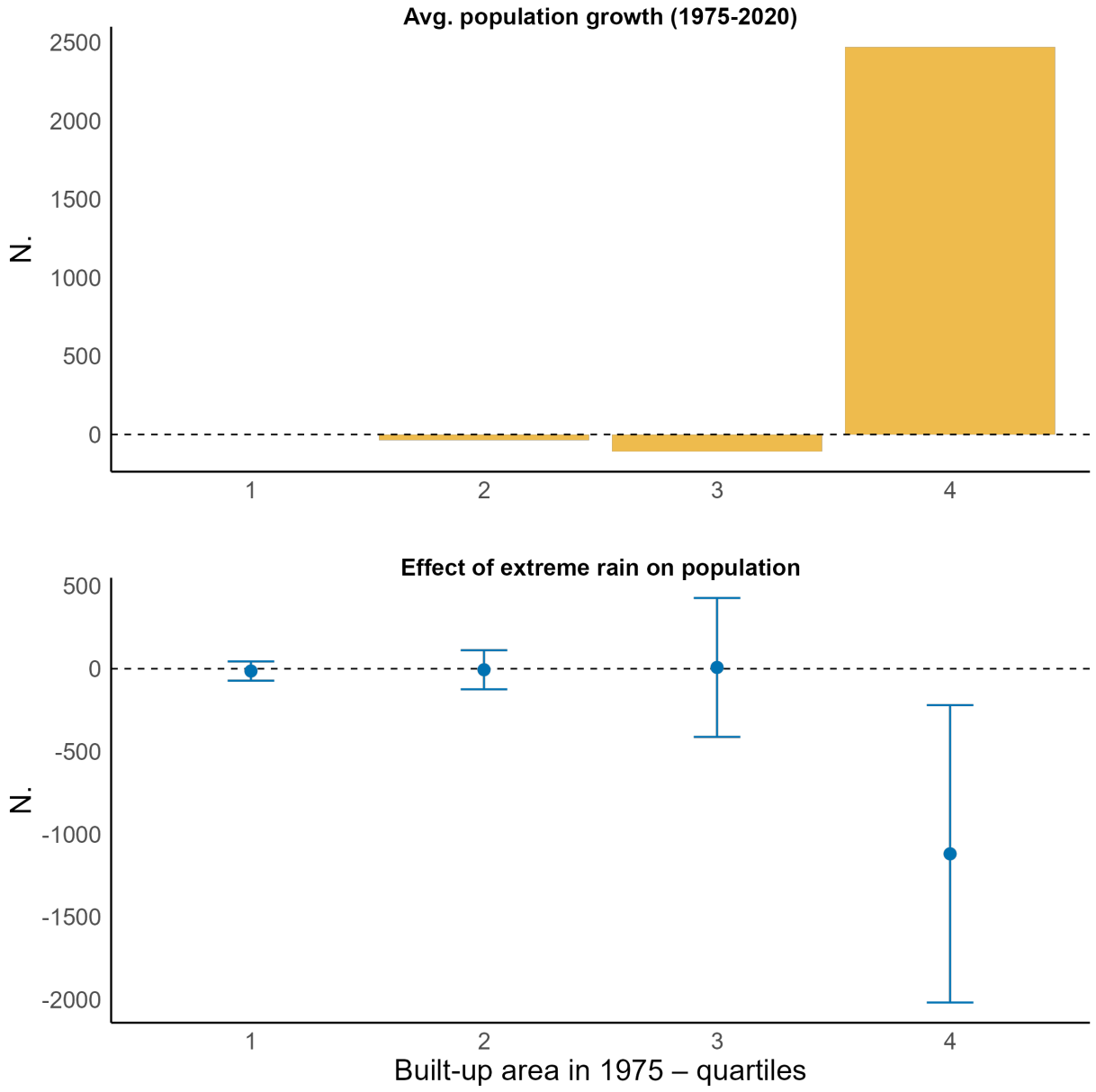

Figure 9: Top: change in population between 1975 and 2020, by quartile of built-up area in 1975. **Bottom**: effect of extreme precipitation (1 additional day above 99.9th percentile) on population, by quartile for built-up area in 1975. Effects are estimated by adding interaction terms to the SFD version of the long-difference model in Equation (3), with added interaction terms for quartile of built-up area. Bands indicate 95% confidence intervals.

Risk and income

In theory, adaptation should be more pronounced in areas with greater exposure to risk and higher levels of income. Figures B.4 and B.5 in the Appendix test these hypotheses. Figure B.4 plots long-difference coefficients and built-up area growth rates by quartile of flood risk, where flood risk is proxied by modelled flood depth in a 1-in-100-year event using data from Dottori et al. (2022). The estimated effects of extreme precipitation on built-up growth are negative and of similar magnitude in the 1st, 3rd, and 4th quartiles, and statistically insignificant in the 2nd quartile. Built-up area growth rates are also relatively stable across quartiles, suggesting limited heterogeneity in development patterns by flood exposure.

Figure B.5 presents the same analysis by quartile of per capita income in 2020. Because income data are available only at the NUTS-3 level and only within the EU, the analysis excludes non-EU regions and loses subregional variation due to the use of SFD. The coefficient on extreme precipitation is significantly negative only in the 3rd income quartile, with no clear pattern across the quartiles.

Taken together, these results offer limited support for the hypothesis that adaptation increases with either flood risk or income. Several factors may account for this. First, the 1-in-100-year flood risk measure captures only fluvial flooding along major rivers and does not reflect flash flood risks caused by extreme precipitation in smaller rivers or urban drainage failures. Second, the risk measure does not account for flood protection infrastructure such as levees, dams, or drainage systems. Finally, higher-income areas typically have more expensive real estate, increasing the opportunity cost of restricting development. Higher income areas may also invest more in flood protection infrastructure, reducing the need to relocate.

5.4 Costs of spatial adaptation

Extreme precipitation can alter where new construction takes place, shifting activity away from locations that would otherwise be preferred. In urban economics, the structure of cities reflects households' trade-offs between proximity to centres and housing space. Climate risks may distort these trade-offs, leading either to higher density in safer areas near centres or to relocation toward more distant, lower-risk sites. This section examines these potential costs of adaptation, focusing

first on spatial spillovers of building activity, and then on changes in density and distance to urban centres. The results provide little evidence that extreme precipitation systematically reshapes these trade-offs.

Spatial spillovers

Extreme precipitation in neighbouring areas can have negative effects on construction if they signal increased flood risk, or positive effects if they lead to reallocation of building activity away from risky areas.

Figure 10 shows spatial effects from the long-difference model with up to six queen–contiguity lags of extreme precipitation.[25] Spatial lags use SFD extreme precipitation (i.e. the difference in extreme precipitation between adjacent cells) rather than raw levels, which lowers spatial correlation. Coefficients are negative for lags 0 and 1, turn positive at intermediate distances, and taper back toward zero for the outermost rings. This pattern suggests that informational and relocation effects coexist: extreme precipitation in or near a cell discourages construction there, whereas extreme precipitation farther away appears to redirect building activity toward the focal cell. The short-lag (negative) effects are precisely estimated, whereas the longer-distance (positive) effects are subject to greater uncertainty.

[25] Under queen contiguity, any cell sharing an edge or a corner with the focal cell is treated as a neighbour; each additional lag adds one concentric ring. At this grid resolution, the sixth-order lag spans roughly 66.6km north–south. Because meridians converge, east–west reach declines with latitude—about 545km near 35°N (southern Italy) and about 240km near 70°N (northern Norway).

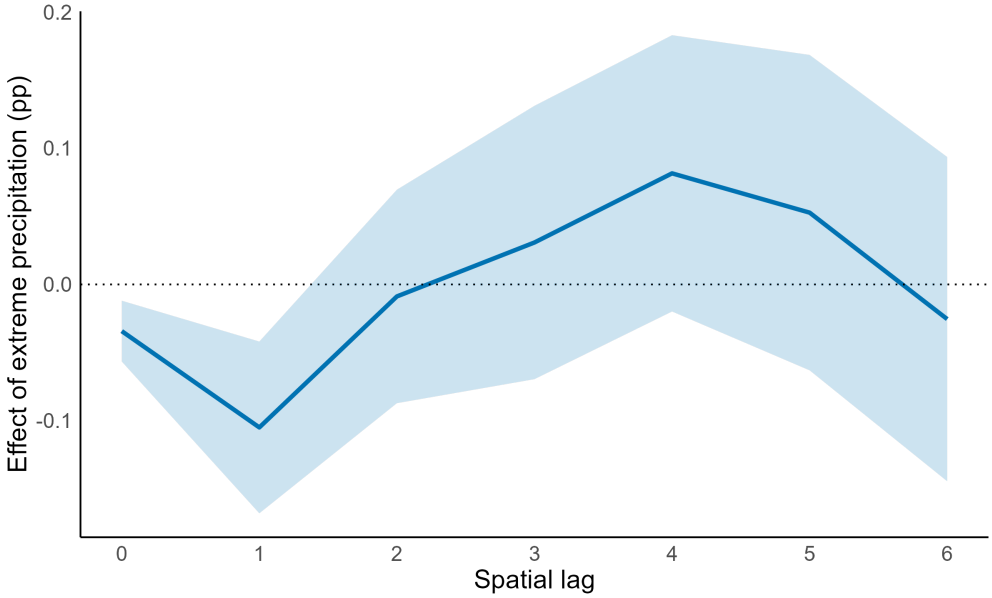

Figure 10: Spatial lags for the effect of extreme precipitation on built-up area. Spatial lag estimates for the change in the number of days with precipitation above the 99.9th percentile using the SFD version of first-difference model in Equation 4. Each spatial lag corresponds to a 0.1° grid cell. 95% confidence intervals.

Urban density

This section tests whether greater exposure to extreme precipitation is associated with residential densification—higher residential share, taller buildings and higher residential density—or instead with changes in the built footprint and population. Using a long-difference with spatial first-differencing design, Tables 3 and 4 report estimates for building use, height and volume, and for population and density at the cell level, using additional data from the Global Human Settlement Layer.

Table 3 shows that one additional extreme-precipitation day (annual average) is associated with a reduction of 0.035 percentage points in residential surface and 0.010 percentage points in non-residential surface. The residential share of the built-up area declines only marginally and is not statistically significant. Average building height changes by 0.009 m (not significant). Building volume falls, consistent with a reduction in occupied surface. Table 4 indicates that population decreases by about 371 persons per cell and by 4.17 persons per km^2; residential density (population per km^2 of built-up area) rises by 535 but the effect is not statistically significant.

Taken together, these results are consistent with population relocation and a contraction of the built footprint in areas with greater exposure to extreme precipitation, with little evidence of vertical densification.

Table 3: Effect of extreme precipitation on building use, building height and volume. Long difference model with SFD

	Δ Residential (1)	Δ Non-residential (2)	Δ Share residential (3)	Δ Height (m) (4)	Δ Volume (m^3) (5)
Δ Extreme-precipitation days	-0.0346***	-0.0101***	-6.78×10^{-6}	0.0094	-273,735.9***
	(0.0108)	(0.0036)	(0.0003)	(0.0059)	(74,122.4)
Climate controls	Yes	Yes	Yes	Yes	Yes
Country fixed effects	Yes	Yes	Yes	Yes	Yes
R^2	0.00630	0.00140	0.04272	0.00123	0.00301
Observations	107,463	107,463	94,050	90,833	107,463

Conley (100km) standard-errors in parentheses
*Signif. Codes: ***: 0.01, **: 0.05, *: 0.1*
Note: residential and non-residential in percentage points.

Table 4: Effect of extreme precipitation on population. Long difference model with SFD.

	Δ Population (1)	Δ Pop. density (pop/km²) (2)	Δ Residential density (pop/km²) (3)
Δ Extreme-precipitation days	-371.3**	-4.167**	534.5
	(170.0)	(1.967)	(380.9)
Climate controls	Yes	Yes	Yes
Country fixed effects	Yes	Yes	Yes
R^2	0.00219	0.00166	0.00167
Observations	107,463	107,463	94,039

Conley (100km) standard-errors in parentheses
*Signif. Codes: ***: 0.01, **: 0.05, *: 0.1*
Note: Residential density is population per square kilometer of residential built-up area.

Distance to urban centres

A potential cost of extreme precipitation is residential relocation away from urban centres, lengthening commuting times. A long-difference SFD model with interactions by 1975 built-up quartiles predicts 2020 population for each grid cell under two cases: (i) the observed change in extreme-precipitation days and (ii) a counterfactual with no change. Predicted levels are added to 1975 baselines, cells are grouped into 5-km bands by distance to the nearest urban centre, and shares are normalised within each case.[26] The two distance profiles are virtually identical over 0–100 km, indicating no economically meaningful reallocation by distance (see Appendix Figure B.6).

5.5 Damage from extreme precipitation

The previous sections showed that extreme precipitation influences where and how much building takes place. The next step is to test whether it also translates into measurable damages, and whether these damages are larger where more built-up area is exposed.

Local climate can influence land-use decisions in different ways, for example through its effects on crop yields (which shape the opportunity cost of land) and on human well-being. To isolate the channel operating through damage to built infrastructure, the analysis focuses on extreme precipitation while controlling for other climate characteristics. The assumption is that, conditional

[26] Urban centres are defined as cities (clusters of cells) with at least 50,000 inhabitants.

on these controls, extreme precipitation affects building activity by causing damage—through physical impacts on buildings and infrastructure. Expectations of such future damage then shift development away from higher-risk areas. A strong mapping from precipitation to damages is not automatic, however, since runoff may be contained by soils, rivers, and sewage networks, and riverine floods can originate upstream.

To validate the damage mechanism, the link between extreme precipitation and major flood disasters is examined at the NUTS-3 level, using DRMKC data described in Section 2. Table 5 reports fixed-effects panel estimates with NUTS-3 and time effects and climate controls, using the model in Equation 5. One additional extreme-precipitation day (per year, averaged over the five-year window) is associated with 0.303 more disaster events (about one-third of the mean of 0.9) and EUR 13.7 million in additional damage (compared with a mean of EUR 12.3 million per region over the window). Columns 3–4 scale outcomes by the built-up share to gauge the role of exposure: coefficients remain large and precisely estimated—0.359 additional events and EUR 7.13 million additional damage per percentage point of built-up area—indicating that regions with more built-up surface suffer greater impacts as more capital is exposed to damage. As a reference point, the mean GDP for NUTS-3 regions in 2020 was EUR 11,326 million.

Table 5: Effects of extreme precipitation: number of events and economic damage.

	N. events	Damage (EUR, 000)	N. events / built-up	Damage / built-up (EUR, 000)
	(1)	(2)	(3)	(4)
Extreme-precipitation days	0.303**	13,661.9**	0.359***	7,126.2***
	(0.109)	(5,530.7)	(0.089)	(1,947.7)
Climate controls	Yes	Yes	Yes	Yes
NUTS fixed effects	Yes	Yes	Yes	Yes
Time fixed effects	Yes	Yes	Yes	Yes
R^2	0.43059	0.20142	0.45187	0.20891
Observations	8,792	8,792	8,792	8,792
Mean dependent	0.932	12,261.5	0.641	5,288.5

Clustered (NUTS & Time) standard-errors in parentheses
*Signif. Codes: ***: 0.01, **: 0.05, *: 0.1*
Notes: Built-up expressed as percentage of cell area. Extreme-precipitation days are those above the 99.9th percentile.

6 Discussion

The estimated effect of an additional day of extreme precipitation on both economic damages and built-up share can be combined to approximate the economic benefit of adaptation. This benefit arises when areas experiencing increases in extreme precipitation subsequently exhibit slower growth in built-up share, thereby reducing exposure and limiting associated damages.

A simple accounting framework can help isolate the role of adaptation. Focusing only on the role of built-up share and extreme precipitation, the economic damages from extreme precipitation can be written as:

$$L_{it} = \phi \cdot B_{it} \cdot R_{it}, \tag{7}$$

where L_{it} denotes damages (losses) in cell i and year t, B_{it} is the built-up share, and R_{it} is the number of extreme precipitation days. The parameter ϕ is the constant marginal damage per percentage point of built-up share per extreme-precipitation day, estimated using Equation 5.

The total change in damages between 1975 and 2020 can be decomposed as:

$$\Delta L_i = \phi \left(B_{i,75} \cdot \Delta R_i + R_{i,75} \cdot \Delta B_i + \Delta B_i \cdot \Delta R_i \right), \tag{8}$$

separating contributions from (a) changes in the frequency of extreme precipitation on the original built-up share in 1975 (extreme-precipitation effect), (b) expansion of built-up share under the baseline climate (built effect), and (c) the location of new development relative to changing extreme precipitation (location effect).[27]

The location effect includes both adaptation and other market- or policy-driven changes in settlement patterns. Adaptation, the endogenous change in built-up share in response to extreme precipitation, is defined as:

$$\Delta B_i^A = \rho_{LD} \cdot \Delta R_i, \tag{9}$$

where ρ_{LD} is the sensitivity of built-up share to changes in extreme precipitation estimated with

[27] $\Delta L_i = \phi \left(B_{i,20} \cdot R_{i,20} - B_{i,75} \cdot R_{i,75} \right) = \phi \left[(B_{i,75} + \Delta B_i)(R_{i,75} + \Delta R_i) - B_{i,75} \cdot R_{i,75} \right]$
$= \phi \left(B_{i,75} \cdot \Delta R_i + R_{i,75} \cdot \Delta B_i + \Delta B_i \cdot \Delta R_i \right)$

the SFD long-difference model (see Equation 3). The residual, unrelated to climate adaptation, location effect $\Delta B_i^{NA} = \Delta B_i - \Delta B_i^A$ reflects other forces (market, policy) that influence the location of built-up shares.

Substituting adaptation into the location term yields a full decomposition of the change in damages:

$$\Delta L_i = \underbrace{\phi \cdot B_{i,75} \cdot \Delta R_i}_{\text{Extreme-precipitation effect}} + \underbrace{\phi \cdot R_{i,75} \cdot \Delta B_i}_{\text{Built effect}} + \underbrace{\phi \cdot \rho \cdot (\Delta R_i)^2}_{\text{Adaptation effect}} + \underbrace{\phi \cdot (\Delta B_i - \rho \cdot \Delta R_i) \cdot \Delta R_i}_{\text{Residual location effect}}. \quad (10)$$

The built effect reflects the expansion of the urban footprint under baseline climate conditions and therefore does not represent adaptation.

The different elements of this decomposition can be calculated using data on extreme precipitation and built-up share (available at the cell level) and estimates for ρ and ϕ. The long-difference specification with SFD yields an estimate of the response of built-up share with respect to changes in extreme precipitation, $\hat{\rho}_{LD} = -0.04$. The subsequent calculations treat this estimate as spatially constant, abstracting from potential heterogeneity related, for example, to the initial built-up share in 1975. Cell-level loss data are not available. Section 5.5 therefore estimates the marginal damage parameter at the NUTS-3 level, obtaining $\hat{\phi} = 7{,}126$ (in thousand EUR). An additional extreme-precipitation day raises damages (over five years) by EUR 7.1 million for each percentage point of built-up share. The cell-level decomposition substitutes this NUTS-3 coefficient for ϕ under the assumption that marginal damage is homogeneous within regions. This assumption may understate intra-regional variation in exposure and asset values.

Table 6 shows that nearly one-half of the mean increase in flood losses between 1975 and 2020 is attributable to the expansion of the urban footprint under the baseline climate (EUR 684,000; 46.9% of the total). A further 26.8% (EUR 392,000) arises from the intensification of extreme-precipitation hazards on the 1975 built environment. Climate-driven location adjustments provide a modest benefit, reducing average losses by 4.8% (EUR 70,000), yet this saving is more than offset by additional exposure generated by other, non-climatic location choices, which increase losses by 31.1% (EUR 454,000). Summing all components yields a net increase of EUR 1.46 million per cell. This compares to an average damage of EUR 13.5 million per NUTS-3 unit over 1980-2020.

Table 6: Decomposition of the change in flood damages between 1975 and 2020.

Component	Value	Share (%)
Extreme-precipitation effect	391.7	26.8
Built effect	684.2	46.9
Adaptation effect	-70.3	-4.8
Residual location effect	453.8	31.1
Total change	1459.5	100.0

The adaptation effect is given by the product $\phi \cdot \rho \cdot (\Delta R_i)^2$, which is negative in every cell because $\rho < 0$ and $\Delta R_i^2 > 0$. When the frequency of extreme-precipitation days rises, construction slows or retreats in higher-risk cells, so exposure declines and expected losses fall relative to a fixed-exposure baseline. When the frequency falls, construction shifts toward safer cells, again lowering expected losses by relocating assets away from risk. In both cases, the adaptation term captures the reduction in damages achieved by matching the spatial distribution of buildings to the new pattern of flood risk. Figure 11 shows that most of this benefit arises in cells where extreme-precipitation frequency increases, although gains are also realised where the frequency decreases.

The shape of this relationship recalls the hump-shaped profit functions in Deschênes and Greenstone (2012), where farm profits are maximised at an optimal temperature and fall on either side as conditions deviate. The crucial difference is that profits reflect outcomes before adaptation, while our measure captures the gains after adaptation. In Deschênes and Greenstone (2012), given the production function (Crop 1 in their Figure 2) weather deviations reduce profits directly through lower productivity. The larger the deviation, the larger the benefit of adapting by switching to a more heat-resistant crop (Crop 2). Similarly, in our setting, weather deviations increase the scope for avoided damages because adaptation reallocates construction away from risk.

The shape of this relationship resembles the hump-shaped profit functions in Deschênes and Greenstone (2012) (reproduced in Figure C.7 in the Appendix), where profits for a fixed crop are maximised at an optimal temperature and fall as conditions deviate. In that setting, the envelope of the profit functions is the profit for the optimal crop at each temperature. The benefit of adaptation is the vertical distance between a fixed-crop curve and the envelope—zero at the optimum and increasing

with the magnitude of the deviation. Analogously, as the climate departs from expectations, the scope for reducing damage by reallocating construction away from risk increases, so the benefits of adaptation are zero at the optimal temperature and grow with the deviation.

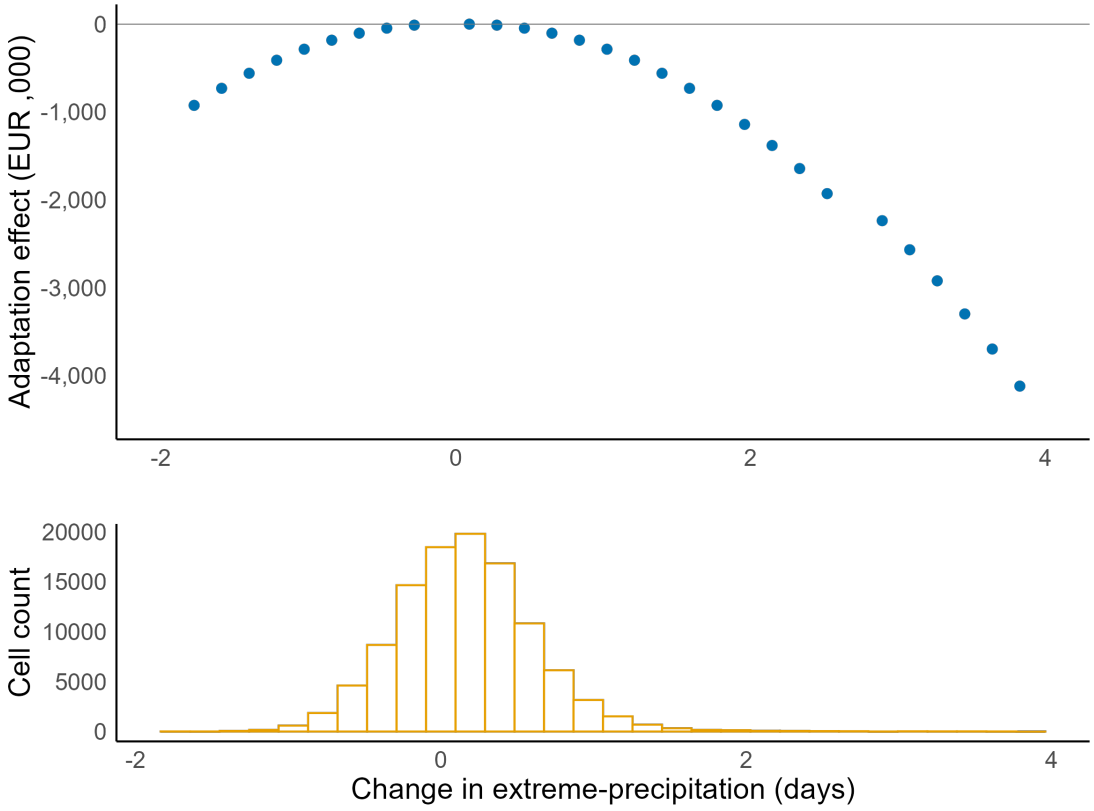

Figure 11: Top: Mean adaptation benefits at the cell level by change in extreme precipitation (average days per year). **Bottom:** Distribution of the change in extreme precipitation.

7 Conclusions

Between 1975 and 2020, both built-up areas and extreme precipitation events increased across Europe. The results presented in this paper indicate that extreme precipitation had a negative impact on local land development. In a context of overall growth in development, building activity relocated away from areas most exposed to extreme precipitation. This adaptation process unfolded gradually over time, consistent with both progressive learning about climate risks and short-term constraints on relocation.

The evidence points to an asymmetry between the costs and benefits of spatial adaptation.

Adjustments in density, commuting distance, or urban form were minimal, suggesting that the costs of adaptation were relatively low. By contrast, the benefits of reduced exposure are substantial, given the strong association between extreme precipitation, built-up share, and flood damages. Several mechanisms may account for this pattern. Adaptation may have occurred along margins not visible in land-use data, such as investments in flood defences, drainage systems, or insurance. These measures reduce damages without requiring relocation and could explain why built-up patterns adjusted only modestly. Relocation within grid cells, for example towards higher ground, could also reduce risk but would not be captured by the estimates.

Another explanation is that adaptation was limited by behavioural or institutional frictions. Individuals may be inattentive to low-probability risks (Maćkowiak and Wiederholt, 2018), expect government assistance in the event of damage (Coate, 1995), or rely on subjective risk perceptions (Bubeck et al., 2012). Relocation costs, such as longer commutes or denser housing, are immediate and salient, while the benefits of lower expected damage are more abstract and harder to evaluate. In such cases, the current pace of adaptation may be suboptimal, providing a rationale for public policy.

The results support a long-term approach to land-use policy. Because adaptation unfolds gradually and is concentrated in areas of growth, policies should focus on steering new development. Relevant instruments include improved flood-risk mapping, zoning that discourages construction in high-risk areas while facilitating development in safer nearby locations, and risk-based insurance schemes. Assessing these options, and identifying the right policy mix, will require additional data on flood maps, insurance markets, and building regulations.

References

Amatulli, G., S. Domisch, M.-N. Tuanmu, B. Parmentier, A. Ranipeta, J. Malczyk, and W. Jetz (2018). A suite of global, cross-scale topographic variables for environmental and biodiversity modeling Background Summary. *Scientific Data* (5), 180040.

Auffhammer, M. (2018). Quantifying economic damages from climate change. *Journal of Economic Perspectives 32*(4), 33–52.

Bakkensen, L. A. and L. Barrage (2022). Going underwater? Flood risk belief heterogeneity and coastal home price dynamics. *Review of Financial Studies 35*(8), 3666–3709.

Bareille, F. and R. Chakir (2023). The impact of climate change on agriculture: A repeat-Ricardian analysis. *Journal of Environmental Economics and Management 119*, 102822.

Barrios, S., L. Bertinelli, and E. Strobl (2010). Trends in rainfall and economic growth in Africa: A neglected cause of the African growth tragedy. *The Review of Economics and Statistics 92*(2), 350–366.

Bernstein, A., S. B. Billings, M. T. Gustafson, and R. Lewis (2022). Partisan residential sorting on climate change risk. *Journal of Financial Economics 146*(3), 989–1015.

Bilal, A. and E. Rossi-Hansberg (2023). Anticipating climate change across the United States. SSRN Working Paper 4475921.

Bubeck, P., W. J. W. Botzen, and J. C. J. H. Aerts (2012). A review of risk perceptions and other factors that influence flood mitigation behavior. *Risk Analysis 32*(9), 1481–1495.

Burke, M. and K. Emerick (2016). Adaptation to climate change: Evidence from u.s. agriculture. *American Economic Journal: Economic Policy 8*(3), 106–140.

Carleton, T., E. Duflo, K. Jack, and G. Zappalà (2024). Adaptation to climate change. NBER Working Paper 33264.

Castells-Quintana, D., M. Krause, and T. K. J. McDermott (2021). The urbanising force of global warming: The role of climate change in the spatial distribution of population. *Journal of Economic Geography 21*(4), 531–556.

Coate, S. (1995). Altruism, the Samaritan's dilemma, and government transfer policy. *American Economic Review 85*(1), 46–57.

Collalti, D. (2024). The economic dynamics after a flood: Evidence from satellite data. *Environmental and Resource Economics 87*(9), 2401–2428.

Damania, R., S. Desbureaux, and E. Zaveri (2020). Does rainfall matter for economic growth? evidence from global subnational data (1990–2014). *Journal of Environmental Economics and Management 102*, 102335.

Dell, M., B. F. Jones, and B. A. Olken (2012). Temperature shocks and economic growth: Evidence from the last half century. *American Economic Journal: Macroeconomics 4*(3), 66–95.

Deschênes, O. and M. Greenstone (2012). The economic impacts of climate change: Evidence from agricultural output and random fluctuations in weather: Reply. *American Economic Review 102*(7), 3761–3773.

Dottori, F., L. Alfieri, A. Bianchi, J. Skoien, and P. Salamon (2022). A new dataset of river flood hazard maps for Europe and the Mediterranean Basin. *Earth System Science Data 14*(4), 1549–1569.

Druckenmiller, H. and S. M. Hsiang (2018). Accounting for unobservable heterogeneity in cross section using spatial first differences. arXiv preprint 1810.07216.

Faiella, A., T. Antofie, S. Luoni, F. Ríos Díaz, and M. Marín Ferrer (2020). The Risk Data Hub loss datasets. Technical report, European Commission, Joint Research Centre (JRC).

Frame, D. E. (1998). Housing, Natural Hazards, and Insurance. *Journal of Urban Economics 44*(1), 93–109.

Gandhi, S., M. E. Kahn, R. Kochhar, S. V. Lall, and V. Tandel (2022). Adapting to flood risk: Evidence from a panel of global cities. NBER Working Paper No. 30137.

Giglio, S., B. Kelly, and J. Stroebel (2021). Climate finance. *Review of Financial Studies 34*(3), 1556–1580.

Grosset, F., A. Papp, and C. Taylor (2023). Rain follows the forest: Land use policy, climate change, and adaptation. *SSRN Electronic Journal*.

Haylock, M. R., N. Hofstra, A. M. Klein Tank, E. J. Klok, P. D. Jones, and M. New (2008). A European daily high-resolution gridded data set of surface temperature and precipitation for 1950-2006. *Journal of Geophysical Research Atmospheres 113*(20), 1–12.

Henderson, J. V., T. Squires, A. Storeygard, and D. Weil (2018). The global distribution of economic activity: Nature, history, and the role of trade. *Quarterly Journal of Economics 133*(1), 357–406.

Hino, M. and M. Burke (2021). The effect of information about climate risk on property values. *Proceedings of the National Academy of Sciences of the United States of America 118*(17).

Holtermann, L. (2020). Precipitation anomalies, economic production, and the role of "first-nature" and "second-nature" geographies: A disaggregated analysis in high-income countries. *Global Environmental Change 65*(October 2019), 102167.

Hsiang, S. (2016). Climate econometrics. *Annual Review of Resource Economics 8*(1), 43–75.

Hsiao, A. (2023). Sea level rise and urban adaptation in Jakarta. Working paper.

Jackson, K. (2016). Do land use regulations stifle residential development? Evidence from California cities. *Journal of Urban Economics 91*, 45–56.

Kala, N. (2017). Learning, adaptation and climate uncertainty: Evidence from Indian agriculture. Working paper.

Kocornik-Mina, A., T. K. J. McDermott, G. Michaels, and F. Rauch (2020). Flooded cities. *American Economic Journal: Applied Economics 12*(2), 35–66.

Kolstad, C. D. and F. C. Moore (2020). Estimating the economic impacts of climate change using weather observations. *Review of Environmental Economics and Policy 14*(1), 1–24.

Kotz, M., A. Levermann, and L. Wenz (2022). The effect of rainfall changes on economic production. *Nature 601*(7892), 223–227.

Lehner, B. and G. Grill (2013). Global river hydrography and network routing: Baseline data and new approaches to study the world's large river systems. *Hydrological Processes 27*(15), 2171–2186.

Lin, Y., T. McDermott, and G. Michaels (2024). Cities and the sea level. *Journal of Urban Economics 143*, 103685.

Linsenmeier, M. (2023). Temperature variability and long-run economic development. *Journal of Environmental Economics and Management 121*, 102840.

Maćkowiak, B. and M. Wiederholt (2018). Lack of preparation for rare events. *Journal of Monetary Economics 100*(1), 35–47.

Magontier, P. and R. Martinez-Mazza (2024). Floods and urban density. Working paper.

Mendelsohn, R. and A. Dinar (2009). Land use and climate change interactions. *Annual Review of Resource Economics 1*(1), 309–332.

Mendelsohn, R., W. D. Nordhaus, and D. Shaw (1994). The impact of global warming on agriculture: A ricardian analysis. *American Economic Review 84*(4), 753–771.

Myhre, G., K. Alterskjær, C. W. Stjern, Hodnebrog, L. Marelle, B. H. Samset, J. Sillmann, N. Schaller, E. Fischer, M. Schulz, and A. Stohl (2019). Frequency of extreme precipitation increases extensively with event rareness under global warming. *Scientific Reports 9*(1), 1–10.

Oh, H., C. Yang, and C. Yoon (2024). Land development and frictions to housing supply over the business cycle. *Finance and Economics Discussion Series 2854*(2024-010), 1–41.

Ospital, A. (2023). Urban policy and spatial exposure to environmental risk. Job market paper.

Pesaresi, M. and P. Politis (2023). GHS-BUILT-S R2023A: GHS built-up surface grid, derived from sentinel-2 composite and landsat, multitemporal (1975–2030). Technical report, European Commission, Joint Research Centre (JRC).

Pesaresi, M., M. Schiavina, P. Politis, S. Freire, K. Krasnodębska, J. H. Uhl, A. Carioli, C. Corbane, L. Dijkstra, P. Florio, et al. (2024). Advances on the Global Human Settlement Layer by joint

assessment of earth observation and population survey data. *International Journal of Digital Earth 17*(1), 2390454.

Rajib, A., Q. Zheng, C. R. Lane, H. E. Golden, J. R. Christensen, I. I. Isibor, and K. Johnson (2023). Human alterations of the global floodplains 1992–2019. *Scientific Data 10*(1), 499.

Taylor, C. A. and H. Druckenmiller (2022, April). Wetlands, flooding, and the clean water act. *American Economic Review 112*(4), 1334–1363.

Wimmer, S., C. Stetter, J. Schmitt, and R. Finger (2024). Farm-level responses to weather trends: A structural model. *American Journal of Agricultural Economics 106*(3), 1241–1273.

Appendix

A Additional summary statistics

A.1 Trends built-up share and extreme precipitation

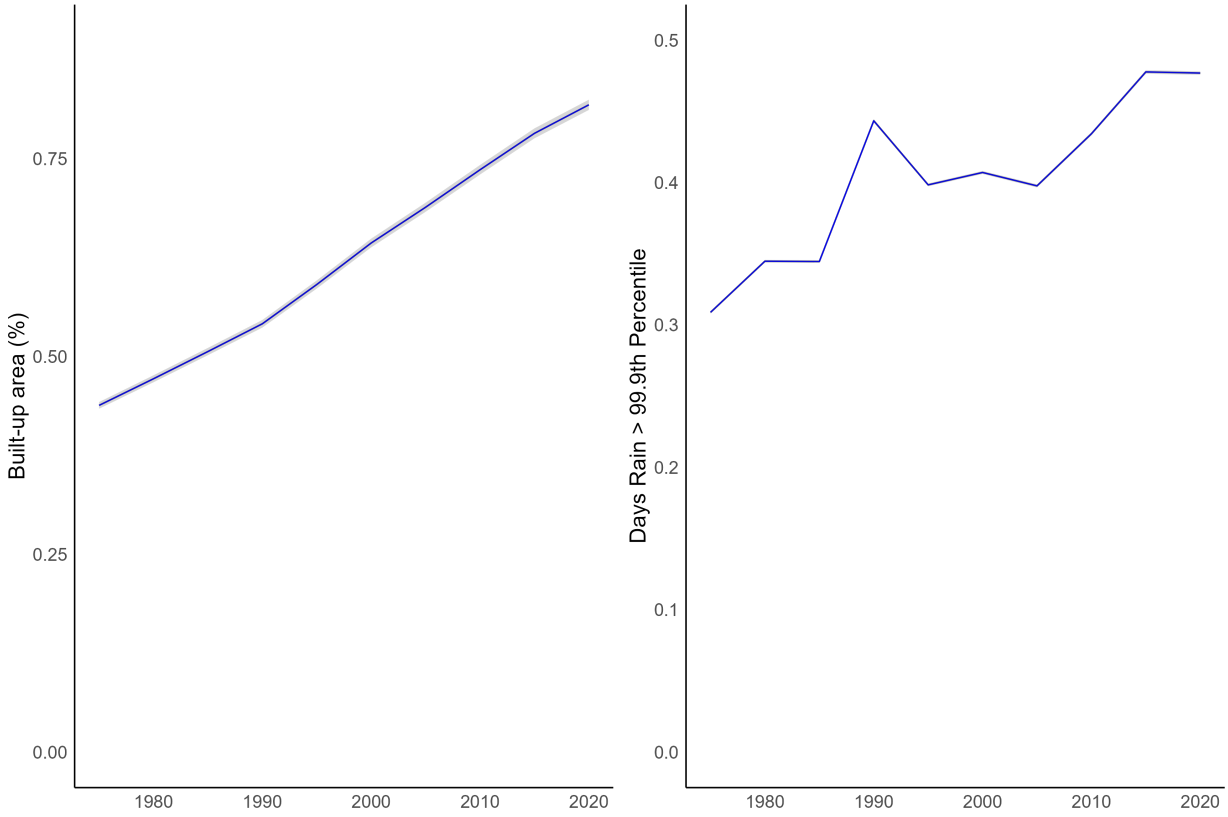

Figure A.1: Built-up share and extreme precipitation in Europe, 1975–2020 (five-year windows). Built-up share is the ratio of built-up area to total cell area. Extreme precipitation is the mean number of days in the window with daily precipitation above the 99.9th percentile threshold, measured for the five-year window ending in each year.

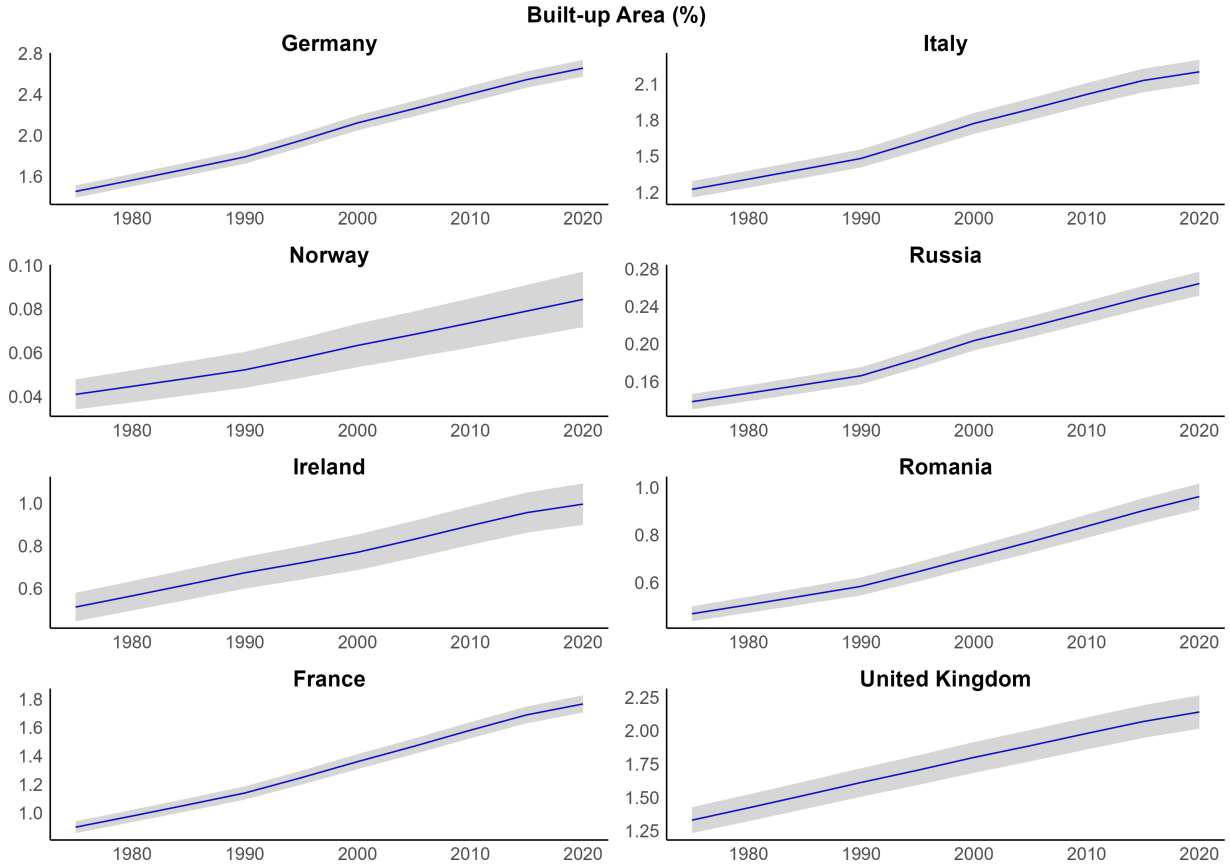

Figure A.2: Built-up share by country, 1975–2020. Built-up share is the ratio of built-up area to total cell area (per cent).

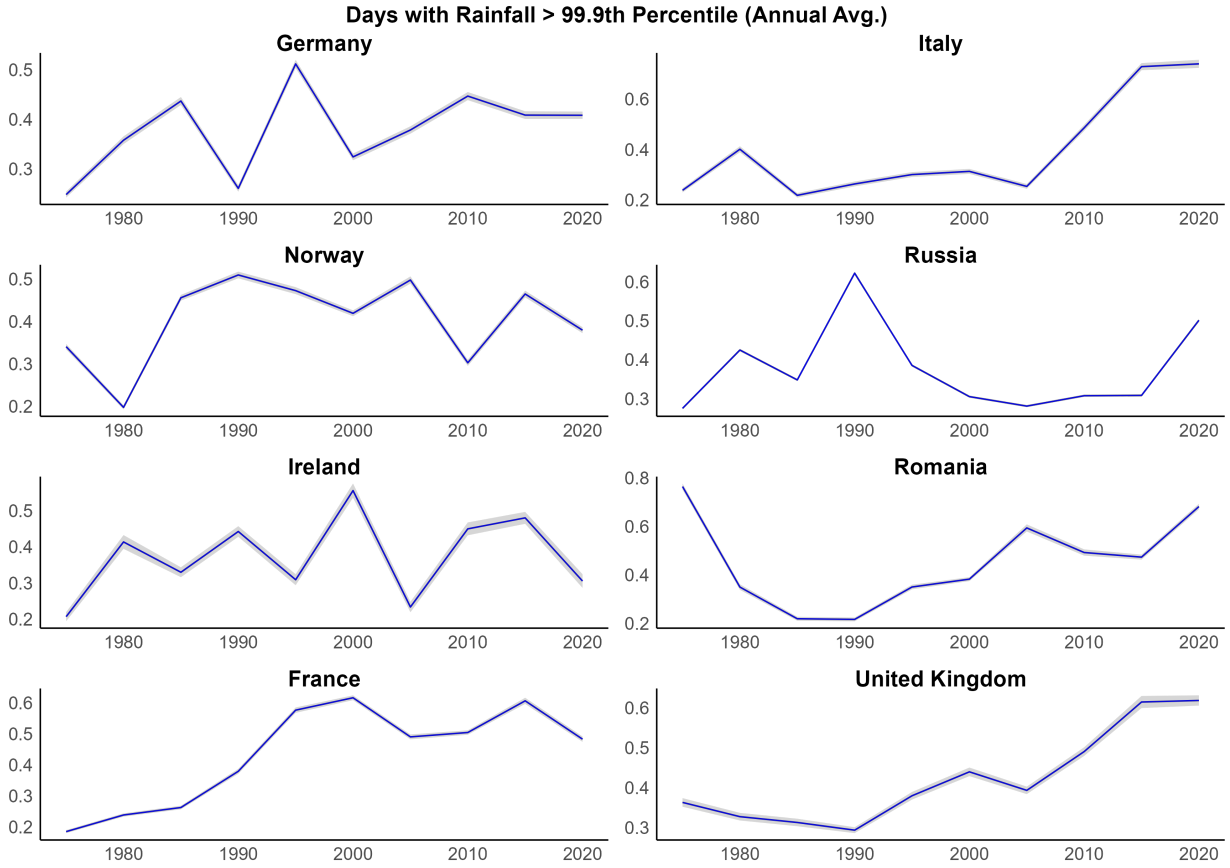

Figure A.3: Extreme precipitation by country, 1975–2020 (annual averages). Each panel shows the annual average number of days with daily precipitation above the 99.9th-percentile threshold.

Table A.1: Summary statistics, cross-sectional model.

Variable	Mean	SD	Min	Max	Median	N. Obs
Built surface (%)	0.82	1.89	0.00	55.52	0.170	108,873
Days with precipitation > 99.9th pct.	0.45	0.18	0.00	1.35	0.450	108,873
Elevation (m)	460.11	526.57	1.00	5,625.00	239.000	108,873
Roughness	81.23	95.82	0.00	905.50	40.000	108,873
Slope (%)	10.92	11.02	0.00	67.60	6.150	108,873
River discharge (m^3/s)	43.48	301.62	0.00	8,241.00	1.740	108,873
Number of rivers	6.56	3.89	0.00	58.00	6.000	108,873
Distance to urban centre (km)	96.12	94.34	0.00	632.95	61.190	108,873
Annual precipitation (mm)	692.05	288.72	187.06	3,711.80	613.500	108,873
Annual precipitation^2	584,938.81	724,768.22	38,164.62	14,119,050.00	388,724.970	108,873
Rainy days	118.72	29.94	25.20	243.30	121.300	108,873
Rainy days^2	15,347.21	7,589.07	750.50	59,481.90	15,066.450	108,873
Monthly precipitation deviations	0.03	0.10	-0.54	0.81	0.030	108,873
Monthly precipitation deviations^2	0.15	0.14	0.03	1.48	0.110	108,873
Δ Mean temperature	0.91	0.29	-1.53	2.37	0.930	108,873
Mean temp. $\times$ Δ Mean temp.	6.33	4.34	-26.41	33.56	5.990	108,873
Mean temperature (°C)	7.36	4.32	-7.77	19.70	7.740	108,873
Temperature variability	4.00	0.73	1.83	6.35	4.050	108,873

Table A.2: Summary statistics, long-difference model.

Variable	Mean	SD	Min	Max	Median	N. Obs
Δ Built surface (p.p.)	0.38	0.77	0.00	31.40	0.07	108,873
Δ Days with precipitation > 99.9th pct.	0.17	0.48	-1.80	3.80	0.20	108,873
Δ Annual precipitation (mm)	25.12	176.37	-1,771.20	1,289.74	38.02	108,873
Δ Annual precipitation^2	50,247.36	335,708.40	-3,894,087.19	6,590,052.00	43,012.56	108,873
Δ Rainy days	-0.97	23.81	-213.80	83.20	1.60	108,873
Δ Rainy days^2	197.01	5,000.49	-56,814.60	25,049.60	329.20	108,873
Δ Monthly precipitation deviations	0.09	0.38	-2.30	1.49	0.11	108,873
Δ Monthly precipitation deviations^2	0.11	0.47	-1.07	4.16	0.01	108,873
Δ(Δ Mean temperature)	-0.35	0.86	-3.27	2.42	-0.21	108,873
Mean temp. × Δ(Δ Mean temp.)	1.01	5.40	-46.24	36.83	0.53	108,873
Δ Mean temperature (°C)	1.36	0.52	-2.64	4.49	1.36	108,873
Δ Temperature variability	-0.12	0.29	-2.26	2.97	-0.04	108,873

Table A.3: Summary statistics, first-difference model.

Variable	Mean	SD	Min	Max	Median	N. Obs
Δ Built surface (p.p.)	0.05	0.10	0.00	9.22	0.01	849,573
Δ Days with precipitation > 99.9th pct.	0.02	0.42	-5.20	5.20	0.00	1,038,367
Δ Annual precipitation (mm)	3.31	95.83	-2,318.28	1,875.84	4.68	1,038,367
Δ Annual precipitation^2	6,417.76	219,468.11	-6,528,321.44	7,370,493.00	5,615.50	1,038,367
Δ Rainy days	0.15	11.54	-192.40	156.60	0.40	1,038,367
Δ Rainy days^2	74.38	2,743.08	-50,268.80	40,388.00	85.60	1,038,367
Δ Monthly precipitation deviations	0.01	0.24	-2.41	1.63	0.01	1,038,367
Δ Monthly precipitation deviations^2	0.01	0.15	-2.35	3.98	0.00	1,038,367
Δ(Δ Mean temperature)	0.04	0.99	-4.73	6.54	0.02	943,970
Mean temp. × Δ(Δ Mean temp.)	0.24	5.61	-73.65	76.24	0.17	943,970
Δ Mean temperature (°C)	0.17	0.55	-3.18	3.36	0.22	1,038,367
Δ Temperature variability	-0.03	0.22	-2.64	2.80	-0.03	1,038,367

B Additional results

Table B.4: Cross sectional model: effect of extreme precipitation on built-up share.

	Built-up	
	Levels	SFD
	(1)	(2)
Extreme-precipitation days	-0.4547***	-0.4461***
	(0.1535)	(0.0843)
Elevation (m)	-0.0006***	0.0002**
	(0.0001)	(7.99×10^{-5})
Roughness	-0.0003	-0.0010***
	(0.0007)	(0.0002)
Slope (%)	0.0104	0.0052**
	(0.0067)	(0.0023)
River discharge (m^3/s)	0.0004***	0.0003***
	(0.0001)	(7.21×10^{-5})
Number of rivers	0.0340***	0.0213***
	(0.0039)	(0.0020)
Distance to urban center (km)	-0.0024***	-0.0483***
	(0.0005)	(0.0034)
Annual precipitation (mm)	0.0007	0.0038***
	(0.0006)	(0.0011)
Annual precipitation^2 (mm)	-1.82×10^{-7}	-9.82×10^{-7}***
	(1.56×10^{-7})	(2.82×10^{-7})
Rainy days	0.0134	-0.1590***
	(0.0095)	(0.0200)
Rainy days^2	-8.96×10^{-5}**	0.0003***
	(3.5×10^{-5})	(7.61×10^{-5})
Monthly precipitation deviations	0.0764	2.103***
	(0.2595)	(0.4421)
Monthly precipitation deviations^2	0.3261	-1.660***
	(0.3104)	(0.5344)
Delta mean temperature	0.6623***	1.228***
	(0.1882)	(0.3747)
Mean temp. × Delta mean temp.	-0.0689**	-0.1219***
	(0.0272)	(0.0380)
Mean temperature (°C)	0.0904**	0.2603***
	(0.0452)	(0.0489)
Temperature variability	0.0105	0.9857***
	(0.0892)	(0.2576)
Country fixed effects	Yes	Yes
Observations	108,070	106,668
R^2	0.25297	0.07344
Within R^2	0.07286	0.07297
Mean share built-up area (%)	0.8177	-0.0006

Conley (100km) standard-errors in parentheses
*Signif. Codes: ***: 0.01, **: 0.05, *: 0.1*

Note: Extreme-precipitation days: days with precipitation > 99.9th percentile. Climate variables: means for 2000-2020. Built-up share: 2020.

Table B.5: Long difference model: effect of extreme precipitation on built-up share.

	Δ Built-up	
	Levels	SFD
	(1)	(2)
Δ Extreme-precipitation days	-0.0614**	-0.0400***
	(0.0252)	(0.0116)
Δ Annual precipitation (mm)	-0.0004	-0.0006
	(0.0005)	(0.0006)
Δ Annual precipitation^2 (mm)	1.9×10^{-8}	-3.33×10^{-8}
	(1.06×10^{-7})	(1.02×10^{-7})
Δ Rainy days	0.0060	0.0100*
	(0.0055)	(0.0059)
Δ Rainy days^2	-2.6×10^{-5}	-4.6×10^{-5}**
	(1.8×10^{-5})	(2.08×10^{-5})
Δ Monthly precipitation deviations	0.0916	0.1905
	(0.1281)	(0.2069)
Δ Monthly precipitation deviations^2	0.0103	0.0375
	(0.0632)	(0.0794)
Δ_t Mean temperature -		
Δ_{t-1} Mean temperature	0.1175***	-0.1293
	(0.0283)	(0.1393)
Δ_t(Mean temp. $\times$ Δ_{t-1} Mean temp.)	0.0010	0.0447**
	(0.0047)	(0.0182)
Δ Mean temperature (°C)	-0.0798*	-0.3489***
	(0.0419)	(0.0785)
Δ Temperature variability	0.1288***	-0.0424
	(0.0470)	(0.0979)
Country fixed effects	Yes	Yes
R^2	0.26887	0.00667
Observations	108,070	106,668
Mean Δ share built-up area (%)	0.3802	-0.0006

Conley (100km) standard-errors in parentheses
*Signif. Codes: ***: 0.01, **: 0.05, *: 0.1*

Note: Extreme-precipitation days: days with precipitation > 99.9th percentile. Climate variables: differences between 2015-2020 vs 1970-1975. Built-up share: difference between 2020 and 1975.

Table B.6: First difference model: effect of extreme precipitation on built-up share.

	Δ Built-up	
	Levels	SFD
	(1)	(2)
Δ Extreme-precipitation days	0.0005	-0.0007***
	(0.0006)	(0.0002)
Δ Annual precipitation (mm)	-1.45×10^{-5}	-3.31×10^{-5}
	(1.33×10^{-5})	(2.09×10^{-5})
Δ Annual precipitation^2 (mm)	1.93×10^{-9}	1.84×10^{-9}
	(2.55×10^{-9})	(3.28×10^{-9})
Δ Rainy days	0.0003**	0.0003**
	(0.0001)	(0.0002)
Δ Rainy days^2	-1.25×10^{-6}**	-1.64×10^{-6}***
	(5.31×10^{-7})	(5.82×10^{-7})
Δ Monthly precipitation deviations	0.0008	0.0073
	(0.0034)	(0.0063)
Δ Monthly precipitation deviations^2	0.0010	-0.0016
	(0.0021)	(0.0028)
Δ_t Mean temperature -		
Δ_{t-1} Mean temperature	0.0034***	0.0137**
	(0.0011)	(0.0060)
Δ_t(Mean temp. $\times$ Δ_{t-1} Mean temp.)	3.41×10^{-5}	0.0004*
	(6.35×10^{-5})	(0.0002)
Δ Mean temperature (°C)	-0.0084***	-0.0336***
	(0.0026)	(0.0108)
Δ Temperature variability	0.0012	-0.0101
	(0.0015)	(0.0072)
Country fixed effects	Yes	Yes
Time fixed effects	Yes	Yes
R^2	0.19933	0.00094
Observations	849,573	806,769
Mean Δ share built-up area (%)	0.0483	-0.0001

Conley (100km) standard-errors in parentheses
*Signif. Codes: ***: 0.01, **: 0.05, *: 0.1*

Note: Extreme-precipitation days: days with precipitation > 99.9th percentile. First differences at 5-year intervals (1975-2020). Climate variables: differences based on 5-year means. Built-up share: differences between end-period values.

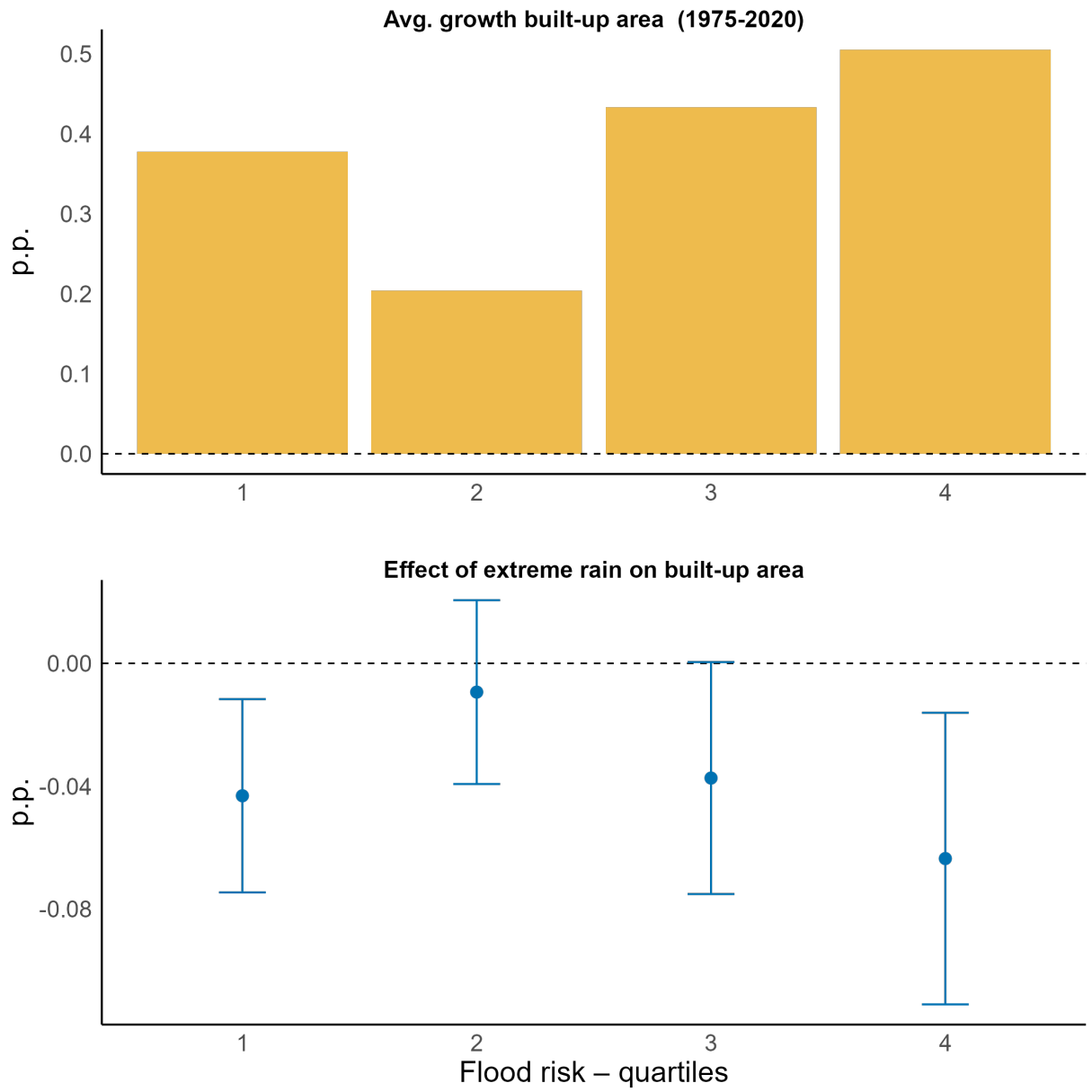

Figure B.4: Top: change in built-up area between 1975 and 2020, by flood risk quartile, measured as flood depth in a 1-in-100 year river flood event. **Bottom**: effect of extreme precipitations (1 additional day above 99.9th percentile) on population, by flood risk quartile. Effects are estimated by adding interaction terms to the SFD version of the long-difference model in equation (3), with an added interaction terms for flood risk quartile. Bands indicate 95% confidence intervals.

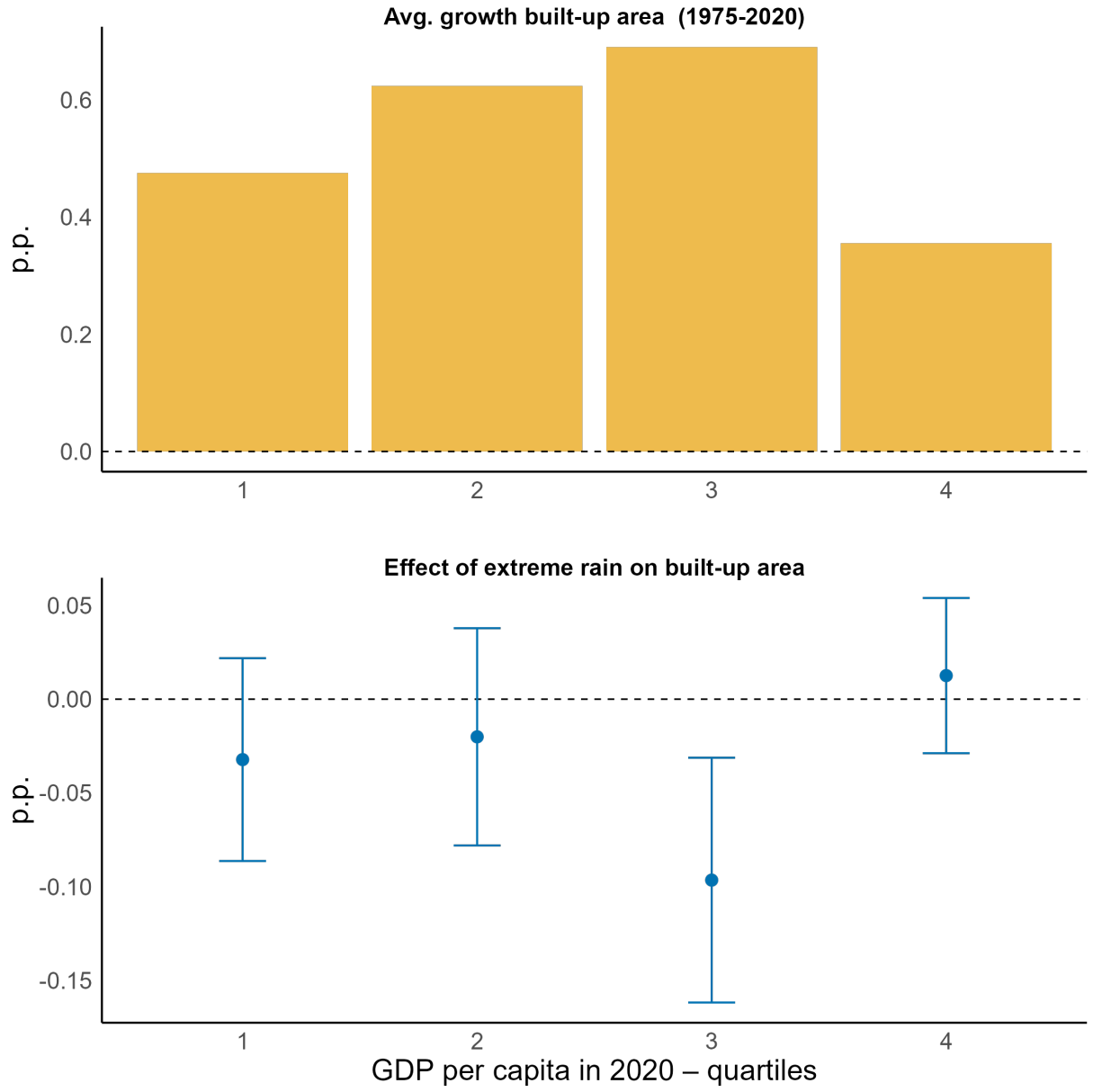

Figure B.5: Top: change in built-up area between 1975 and 2020, by quartile of per-capita income at regional (NUTS-3) level. **Bottom**: effect of extreme precipitations (1 additional day above 99.9th percentile) on population, by per-capita income quartile. Effects are estimated by adding interaction terms to the SFD version of the long-difference model in equation (3), with an added interaction terms for GDP quartile. Bands indicate 95% confidence intervals.

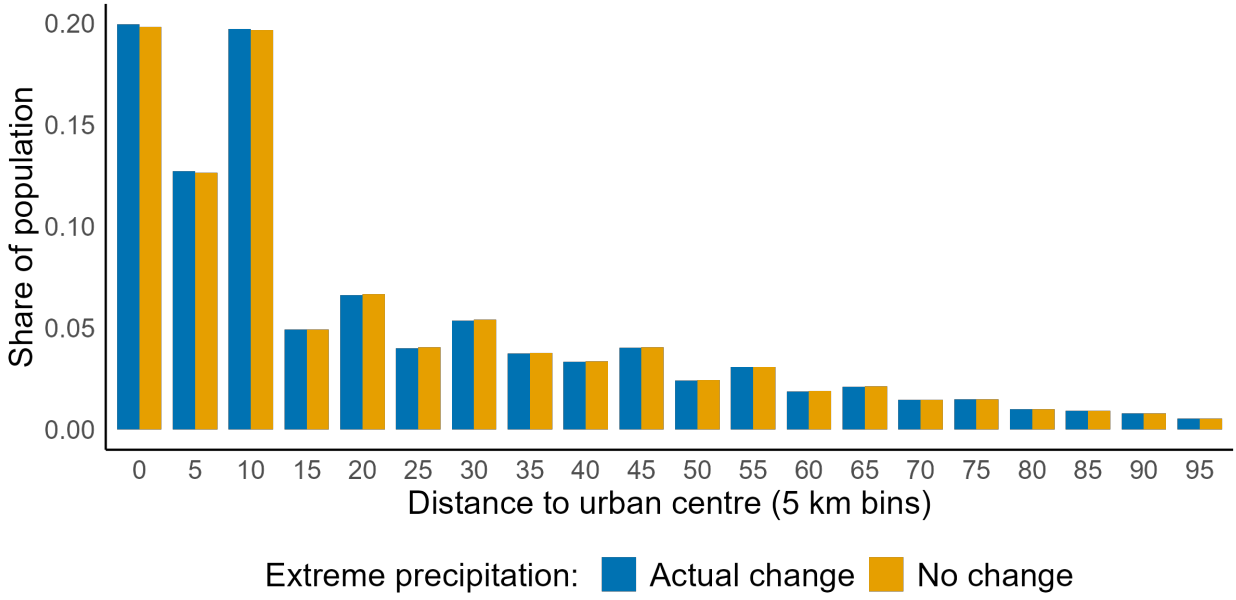

Figure B.6: Population shares by distance to the nearest urban centre under observed changes in extreme-precipitation days and under a counterfactual with no change. Estimates with SFD long-difference model. Shares are computed in 5-km bins and normalised to one in each scenario.

C Benefits of adaptation

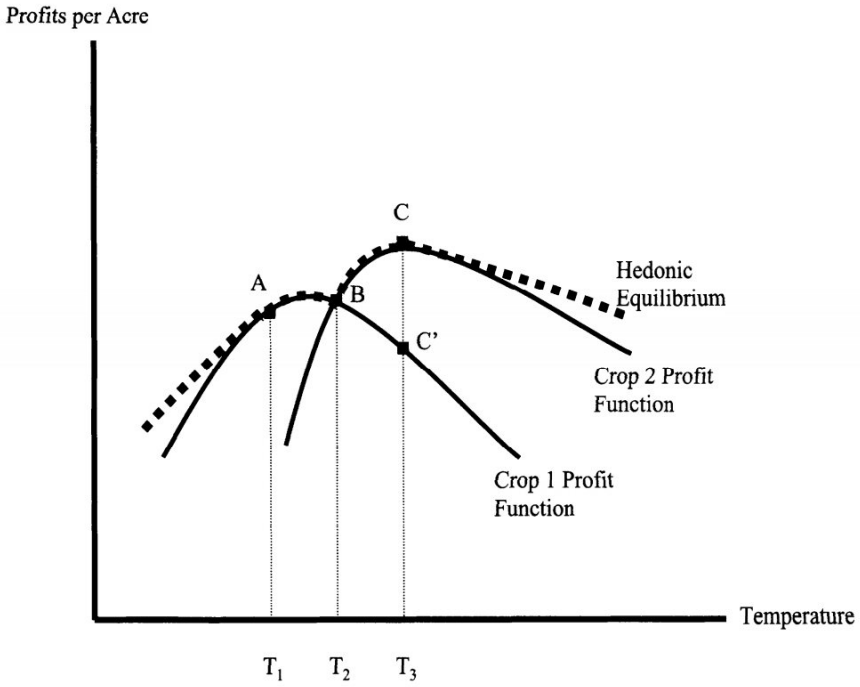

FIGURE 2. THEORETICAL RELATIONSHIP BETWEEN PROFITS PER ACRE AND TEMPERATURE

Figure C.7: Reproduction of Figure 2 from Deschênes and Greenstone (2012)